Surface faulting and paleoseismic history of the 1932 Cedar Mountain earthquake area, west-central Nevada, and implications for modern tectonics of the Walker Lane

John W. Bell*
Craig M. dePolo
Alan R. Ramelli
Nevada Bureau of Mines and Geology, University of Nevada, Reno, Reno, Nevada 89557

Andrei M. Sarna-Wojcicki
C. E. Meyer
U.S. Geological Survey, 345 Middlefield Road, Menlo Park, California 94025

ABSTRACT

The 1932 Cedar Mountain earthquake (M_s 7.2) was one of the largest historical events in the Walker Lane region of western Nevada, and it produced a complicated strike-slip rupture pattern on multiple Quaternary faults distributed through three valleys. Primary, right-lateral surface ruptures occurred on north-striking faults in Monte Cristo Valley; small-scale lateral and normal offsets occurred in Stewart Valley; and secondary, normal faulting occurred on north-northeast–striking faults in the Gabbs Valley epicentral region. A reexamination of the surface ruptures provides new displacement and fault-zone data: maximum cumulative offset is estimated to be 2.7 m, and newly recognized faults extend the maximum width and end-to-end length of the rupture zone to 17 and 75 km, respectively.

A detailed Quaternary allostratigraphic chronology based on regional alluvial-geomorphic relationships, tephrochronology, and radiocarbon dating provides a framework for interpreting the paleoseismic history of the fault zone. A late Wisconsinan alluvial-fan and piedmont unit containing a 32–36 ka tephra layer is a key stratigraphic datum for paleoseismic measurements.

Exploratory trenching and radiocarbon dating of tectonic stratigraphy provide the first estimates for timing of late Quaternary faulting along the Cedar Mountain fault zone. Three trenches display evidence for six faulting events, including that in 1932, during the past 32–36 ka. Radiocarbon dating of organic soils interstratified with tectonically ponded silts establishes best-fit ages of the pre-1932 events at 4, 5, 12, 15, and 18 ka, each with ±2 ka uncertainties. On the basis of an estimated cumulative net slip of 6–12 m for the six faulting events, minimum and maximum late Quaternary slip rates are 0.2 and 0.7 mm/yr, respectively, and the preferred rate is 0.4–0.5 mm/yr. The average recurrence (interseismic) interval is 3600 yr. The relatively uniform thickness of the ponded deposits suggests that similar-size, characteristic rupture events may characterize late Quaternary slip on the zone. A comparison of event timing with the average late Quaternary recurrence interval indicates that slip has been largely regular (periodic) rather than temporally clustered.

To account for the spatial separation of the primary surface faulting in Monte Cristo Valley from the epicenter and for a factor-of-two-to-three disparity between the instrumentally and geologically determined seismic moments associated with the earthquake, we hypothesize two alternative tectonic models containing undetected subevents. Either model would adequately account for the observed faulting on the basis of wrench-fault kinematics that may be associated with the Walker Lane.

The 1932 Cedar Mountain earthquake is considered an important modern analogue for seismotectonic modeling and estimating seismic hazard in the Walker Lane region. In contrast to most other historical events in the Basin and Range province, the 1932 event did not occur along a major range-bounding fault, and no single, throughgoing basement structure can account for the observed rupture pattern. The 1932 faulting supports the concept that major earthquakes in the Basin and Range province can exhibit complicated distributive rupture patterns and that slip rate may not be a reliable criterion for modeling seismic hazard.

INTRODUCTION

Background

The December 21, 1932, Cedar Mountain earthquake (M_s 7.2) was a strike-slip event that produced widely distributed, en echelon surface ruptures along a discontinuous zone crossing three valleys of west-central Nevada (Gianella and Callaghan, 1934a; Fig. 1, A and B). The epicenter was originally placed about 10 km north of Cedar Mountain by Gianella and Callaghan (1934a), but it was later more precisely relocated in Gabbs Valley at the northern end of the rupture zone (Byerly, 1935). Doser (1988) used waveform modeling and first-motion data to identify a second subevent and to firmly establish a strike-slip focal mechanism for the main event. The 1932 rupture zone lies within a semicontinuous, north-trending band of historical seismicity and surface faulting commonly referred to as the central Nevada seismic belt (cf. Wallace, 1984; Fig. 1A), and the northern end of the rupture zone overlaps with surface faulting later produced by the 1954 Fairview Peak event (M_s 7.2).

Gianella and Callaghan (1934a) mapped the

*E-mail: jbell@equinox.unr.edu.

Data Repository item 9949 contains additional material related to this article.

GSA Bulletin; June 1999; v. 111; no. 6; p. 791–807; 10 figures; 3 tables.

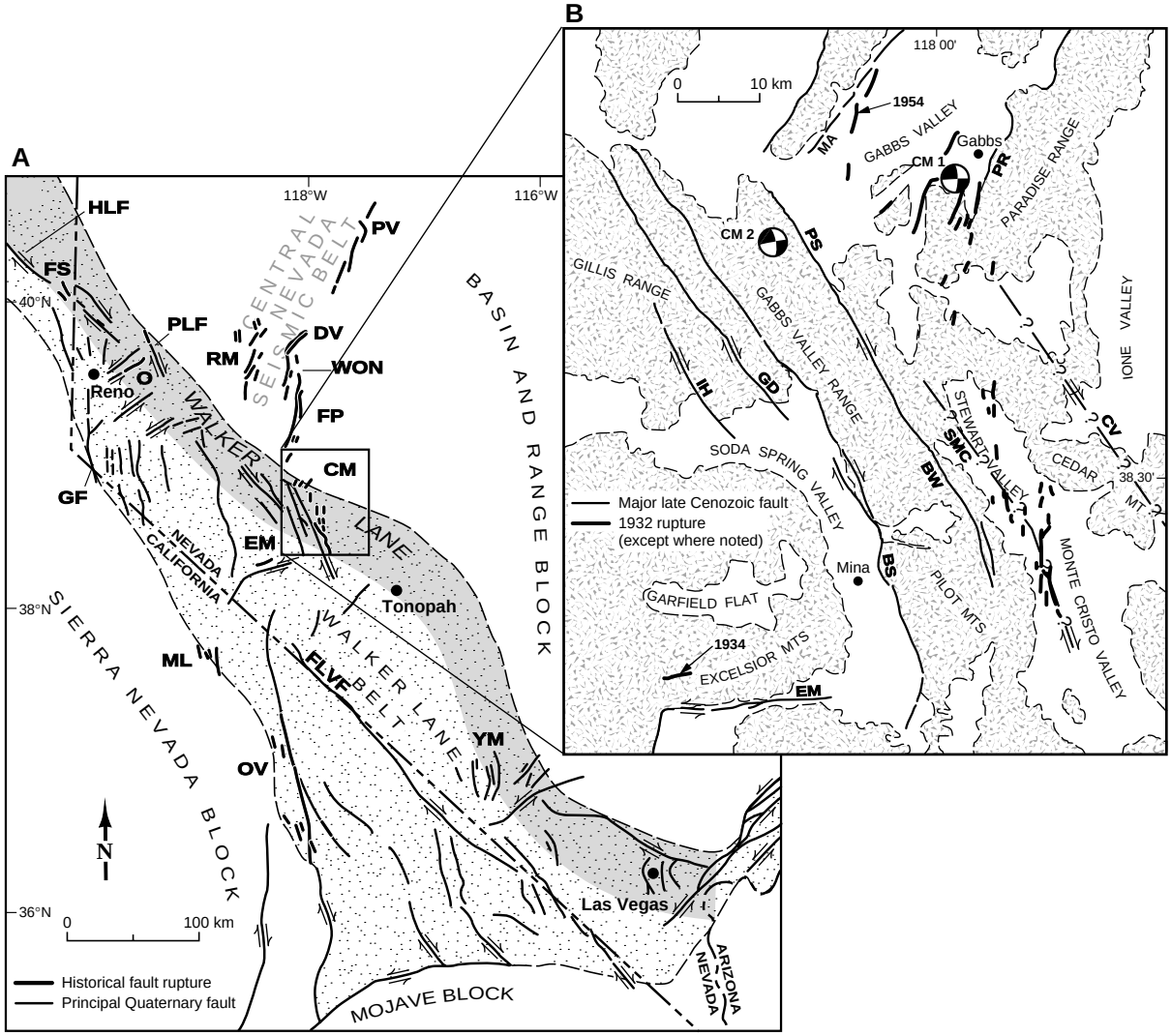

Figure 1. (A) Location map showing historical fault ruptures, principal Quaternary faults, and extent of the Walker Lane (shaded) and Walker Lane belt (dot pattern). Historical surface ruptures are shown by bold fault lines in the following locations: O—1869 Olinghouse; OV—1872 Owens Valley; WON—1903 Wonder; PV—1915 Pleasant Valley; CM—1932 Cedar Mountain; EM—1934 Excelsior Mountain; RM—1954 Rainbow Mountain; FP—1954 Fairview Peak; DV—1954 Dixie Valley; FS—1959 Fort Sage; and ML—1986 Mammoth Lakes. Other principal active faults include PLF—Pyramid Lake fault; HLF—Honey Lake fault; GF—Genoa fault; and FLVF—Fish Lake Valley fault. YM—Yucca Mountain. Modified from Stewart (1988). (B) Location map showing distribution of the 1932 Cedar Mountain ruptures (bold lines) and the principal faults of the central Walker Lane: PS—Petrified Spring; BW—Bettles Well; BS—Benton Spring; GD—Gumdrop Hills; IH—Indian Head; EM—Excelsior Mountain; PR—Paradise Range; MA—Mount Annie. SMC—Stewart–Monte Cristo Valley fault of Molinari (1984). CV—Cirac Valley fault of Hardyman et al. (1992). "1934" and "1954" indicate Excelsior Mountain and Fairview Peak ruptures; respectively. Locations and focal mechanisms for the 1932 main event (CM 1) and subevent (CM 2) are from Doser (1988).

rupture zone shortly after the event and documented the principal "rifts" along a set of north-trending, left-stepping structural alignments extending from Monte Cristo Valley northward through Stewart Valley to Gabbs Valley. Owing to the right-lateral, en echelon nature of the ruptures, Gianella and Callaghan (1934b) hypothesized that the 1932 event was illustrative of San Andreas–style faulting along a narrow, northwest-trending structural-physiographic line in western Nevada later named "the Walker Lane." As originally defined (cf. Locke et al., 1940), the Walker Lane is a 700-km-long zone of Cenozoic strike-slip structure and physiography that disrupts the otherwise north-northeast–trending extensional terrain of the Basin and Range province to the east (Fig. 1A). The zone was redefined by Carr (1984) and Stewart (1988) who used the term "Walker Lane belt" to describe a wider range of structures lying between the Sierra Nevada on the west and the original Walker Lane on the east. Here, we limit our discussion to the region originally called the Walker Lane.

The 1932 faulting occurred in the central Walker Lane, a region characterized by N40°W-striking, left-stepping, right-lateral transcurrent faults (Hardyman and Oldow, 1991; Fig. 1B). Post-Oligocene right offset on individual faults is estimated at between 9 and 18 km, with cumula-

tive late Cenozoic right offset across the central Walker Lane estimated to be between 48 and 75 km (Ekren and Byers, 1984; Stewart, 1988).

Gianella and Callaghan (1934b) suggested that the 1932 faulting was due to regional-scale, right-lateral wrench faulting within the Walker Lane. Molinari (1984) mapped late Cenozoic structure in the southern half of the rupture zone and similarly attributed the 1932 ruptures to wrench tectonics. On the basis of modern seismologic and geodetic data, however, Doser (1988) and Savage et al. (1995) concluded that the 1932 event appeared more closely related to the historical behavior of the central Nevada seismic belt that transects the Walker Lane.

Purpose and Scope

The Cedar Mountain earthquake was one of the largest historical events to occur within the Walker Lane region, and it exhibited several complex structural and tectonic relationships that make it an important event for understanding the contemporary tectonics of the western Basin and Range province. Unlike most other historical surface-rupturing earthquakes in the Basin and Range province, the 1932 surface faulting did not occur along a major range-bounding fault but instead along a series of widely distributed, low-relief, midvalley faults. Regional mapping has not identified any single, throughgoing basement structure that could account for the observed rupture and displacement patterns (Whitebread and John, 1982) although several concealed basement faults have been postulated (Fig. 1B; Ekren et al., 1976; Molinari, 1984; Hardyman et al., 1992).

The Cedar Mountain earthquake provides a modern analogue for evaluating seismic hazard in the Walker Lane region. The proposed high-level nuclear waste repository at Yucca Mountain lies within the tectonic framework of the southern part of the region (Fig. 1A; cf. Carr, 1984), and the 1932 earthquake is considered an important event bearing on the seismotectonic setting of the site (U.S. Department of Energy, 1988). Recent studies suggest that fault kinematics in the Yucca Mountain region can be modeled by using regional strike-slip shear relationships found within the Walker Lane (Janssen, 1995; O'Leary, 1996; Fridrich, 1998).

Here, we examine the surface faulting and paleoseismic history of this poorly understood fault zone and attempt to resolve some of the complexities associated with the distributive nature of the 1932 faulting and the apparent lack of a throughgoing basement structure. We synthesize previous mapping of the rupture zone and provide additional new fault-rupture data. Detailed surficial mapping provides new chronostratigraphic data that, combined with results of exploratory trenching, establish the first estimates of timing for late Quaternary faulting in the rupture zone. To better understand the character of seismotectonic processes in the Basin and Range province, we evaluate the complicated fault-rupture pattern. We build on the wrench-fault models proposed by Gianella and Callaghan (1934b) and Molinari (1984), and we speculate on alternative tectonic models that may account for some of the seismologic and fault complexities associated with the earthquake. Last, we discuss the implications of the Cedar Mountain event as it bears on estimating seismic hazard in the Walker Lane region.

SURFACE FAULTING

Approach

Surface faulting accompanying the 1932 earthquake was complexly distributed among three valleys lying east of the northwest-striking transcurrent faults of the Gabbs Valley Range and Pilot Mountains (Fig. 2). Through the use of new low-sun-angle aerial photography at 1:12 000 scale, covering the entire rupture zone, we reviewed and modified the mapping of Gianella and Callaghan (1934a) and Molinari (1984). We evaluated the original field notes of V. P. Gianella (archived at the University of Nevada, Reno) to add further detail to the rupture-zone characteristics. Fault-displacement measurements were made where 1932 offsets were judged to be visible, although observations more than 60 yr after the event involve considerable uncertainty. Here, we combine our measurements with the earlier observations to reconstruct a fairly complete synthesis of surface faulting; we maintain the "rift" identification system of Gianella and Callaghan (1934a). Fault-rupture data were compiled on annotated maps at 1:48 000 scale (available from the Nevada Bureau of Mines and Geology).

Monte Cristo Valley

The largest surface ruptures occurred along a 16-km-long zone in Monte Cristo Valley (Fig. 3), here called the Monte Cristo Valley fault zone. The principal ruptures were linear and uniformly north-trending and exhibited evidence of right offset: displaced gravel bars, left-stepping en echelon scarps, swells, depressions, and moletracks. The most pronounced faulting occurred along a set of late Pleistocene and Holocene traces that display a variety of prominent tectono-geomorphic features, including compound scarps, grabens, pressure ridges, and drainage deflections.

Several large rifts compose the zone. One of the longest single ruptures (5.2 km) was rift 24, a N10°W-striking fault trace that exhibited right-lateral displacements of 1–2 m and vertical offsets of 15–30 cm. Horizontal displacements of wash banks, thalwegs, and channel bars are still visible along much of the rift. The northern end of rift 24 splits with a western branch stepping left to rift 23B along a 30-m-high, northwest-trending pressure ridge formed in Quaternary alluvium. As much as 15 cm of reverse slip occurred along the stepover in 1932, a kinematic relationship consistent with restraining-bend geometry of strike-slip faults (cf. Christie-Blick and Biddle, 1985). Two left-stepping, oblique-slip grabens formed parallel to the principal strike-slip fault traces. Rifts 23C and 24A occurred about 1 km west of rift 24 and had up to 1.7 m of right slip.

Stewart Valley

Small-displacement (1–50 cm) ruptures generally less than 500 m long occurred in Stewart Valley and along the northern and northwestern flanks of Cedar Mountain (Fig. 2). Stewart Valley is a structurally complex basin underlain by Tertiary sedimentary rocks mostly concealed by a thin cover of Quaternary alluvium. Folding within the Tertiary rocks is common and may have accommodated some of the 1932 deformation (Molinari, 1984).

Rifts 13–16 were mapped by Gianella and Callaghan (1934a) as small ground cracks and fissures locally exhibiting components of right offset (Fig. 2). Rift 13A is a previously unmapped, 0.9-km-long fault trace exhibiting a 30–45-cm-high scarp extending through Stewart Springs. We also investigated the 90-cm-high circular scarp (rift 15) reported by Gianella and Callaghan (1934a) surrounding "earthquake hill." On the basis of the pattern of the scarp around the hill and the lack of a visible fault in the underlying Tertiary rocks, we interpret this scarp as a nontectonic, shaking-induced feature.

Gabbs Valley

Surface faulting in Gabbs Valley was distinctly different in style and orientation compared to that in Monte Cristo and Stewart Valleys. Extensional faulting occurred on multiple, widely separated Quaternary faults between the Paradise Range and Mount Annie (Fig. 2). The total cross-strike width of faulting in Gabbs Valley was on the order of 17 km, with interstrike distances between individual breaks ranging from 2 to 13 km.

Rift 0 occurred along the southeastern flank of Mount Annie and was not detected by Gianella and Callaghan (1934a); it was the longest surface break (8 km) in Gabbs Valley with vertical displacements of 20–40 cm and right offsets of up to 80 cm. Rift 0 is located near faulting associated with the 1954 Fairview Peak earthquake, but rift 0

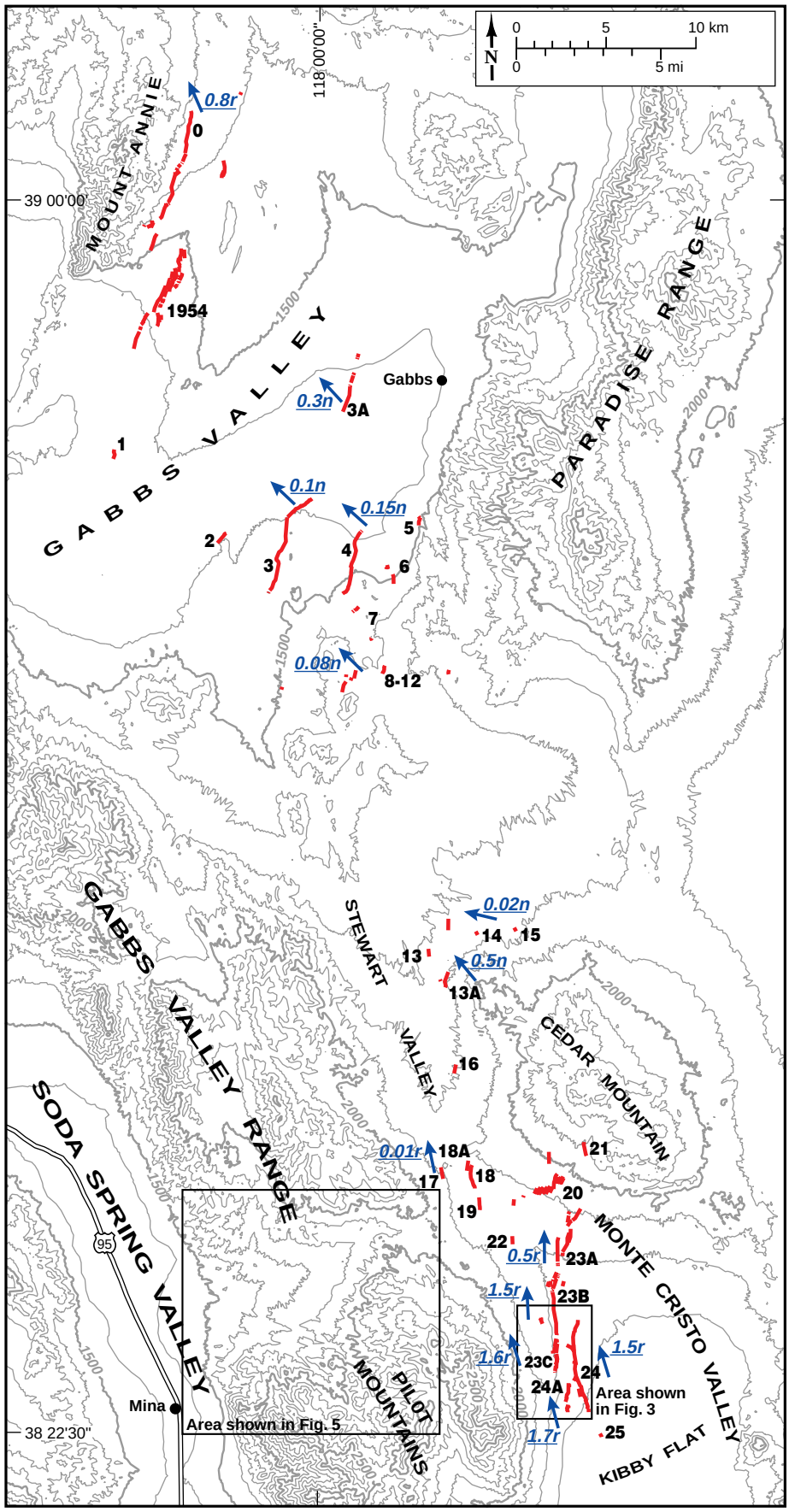

Figure 2. Map showing surface ruptures (red) associated with the 1932 Cedar Mountain earthquake. Rupture numbers correspond to the principal "rifts" of Gianella and Callaghan (1934a), except where numbers were added for newly mapped ruptures (e.g., rift 0). Blue arrows indicate the fault-slip azimuth (horizontal component of net-slip vector) measured across principal ruptures; blue numbers indicate the displacement (in meters) and style of dominant fault displacement (r—right-lateral, n—normal).

scarps are visible on aerial photographs flown prior to the 1954 earthquake and thus cannot be attributed to that event (Caskey et al., 1996). The location of rift 0 indicates that the 1954 Fairview Peak faulting overlapped the 1932 rupture zone by about 14 km.

Several sets of ruptures occurred along the western flanks of fault-controlled bedrock hills at the southern end of the Paradise Range (Fig. 2). Rifts 2, 3, and 4 consisted of 3–5-km-long, 1–15-cm-high, right-stepping, en echelon faults and graben bounding low, north-northeast–trending bedrock hills in the southern part of Gabbs Valley. The previously unmapped rift 3A was 2.2–3.3 km long and had a maximum vertical displacement of 30 cm.

Summary of Surface Faulting

Surface faulting was distributed along a series of left-stepping, north-striking faults and ground cracks forming a rupture zone with an end-to-end length of 75 km and a maximum width of 17 km. Surface displacements showed two distinct populations (Fig. 2): (1) dominantly right-lateral offsets in Monte Cristo Valley having north-trending slip azimuths and (2) dominantly normal offsets in Gabbs Valley having northwest-trending slip azimuths. Faulting in Stewart Valley was a mix of the two sets. The most extensive and largest surface ruptures were in Monte Cristo Valley where the style of faulting was consistent with the right-lateral focal mechanism. Conversely, the small, north-northeast–striking, dominantly normal-slip ruptures in Gabbs Valley corresponded poorly to the main-event mechanism, even though they were spatially closer to the epicenter.

With the largest primary[1] displacements, the Monte Cristo Valley fault zone provides the best sites for measuring coseismic displacements.

[1]Primary surface rupture is defined here as fault displacement interpreted to have a direct connection to subsurface seismogenic slip based on rupture dimensions, displacement, and continuity. Secondary surface rupture has an inferred branching or indirect connection to seismogenic slip.

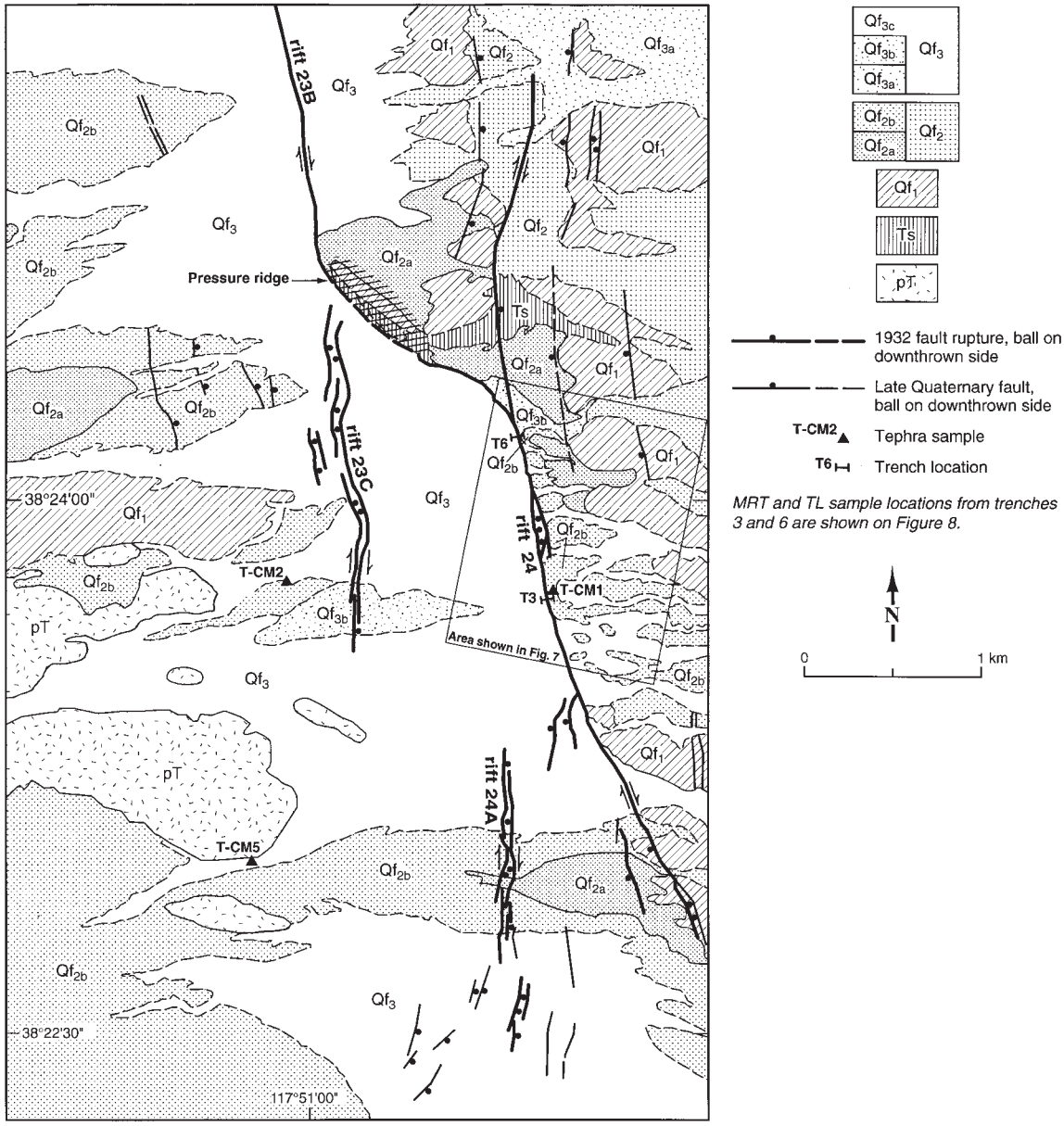

Figure 3. Allostratigraphic map of west-central Monte Cristo Valley showing 1932 fault ruptures (bold), exploratory trench locations, and tephra sample sites. pT—pre-Tertiary rocks; Ts—Tertiary rocks; Qf_1—early and middle Quaternary fan deposits; Qf_2—late Pleistocene fan deposits; Qf_3—late Pleistocene–Holocene fan deposits.

Typical right-lateral displacements measured across individual principal faults ranged between 0.5 and 1.5 m; maximum displacements of 2 m were locally measured on rifts 23C and 24 (Fig. 4). Displacements are summed where faults overlap, and a maximum cumulative displacement is estimated to be 2.7 m on the basis of measurements across rifts 23C and 24. At the stepover pressure ridge between rifts 23C and 24, the cumulative right-lateral displacement was small (<1 m) whereas the vertical displacement was anomalously large (50 cm), a result which suggests that contractional faulting and/or folding accounted for some deformation.

STRATIGRAPHIC, TRENCHING, AND AGE DATA

Stratigraphic Units

Approach. Allostratigraphic mapping of Quaternary surficial deposits provides a chronostratigraphic framework for interpreting the paleoseismic history of the 1932 rupture zone. Allostratigraphic units are similar to alluvial-geomorphic units (Bull, 1991), and they are defined on the basis of the soils and geomorphic surfaces that form the unit boundaries (North American Commission on Stratigraphic Nomenclature, 1983). In constructing detailed allostratigraphic maps for Monte Cristo Valley (Fig. 3) and the adjacent Bettles Well Canyon (Fig. 5; Bell, 1995), we have retained the nomenclature of Molinari (1984).

Quaternary deposits in the Cedar Mountain region are divided into three principal stratigraphic

units (Fig. 6): Qf_1, early to middle Pleistocene fan-piedmont remnants; Qf_2, late Pleistocene fan-piedmont remnants; and Qf_3, late Pleistocene to Holocene fan-piedmont and wash-terrace remnants.

Unit Qf_1. Qf_1 deposits comprise a series of high-level, well-dissected, digitate fan-piedmont remnants (ballenas) lying unconformably on Tertiary sedimentary rocks and older Quaternary fanglomerates. Flat-topped interfluvial remnants, where preserved, contain well-developed, tightly packed desert pavement and dark rock varnish. In Monte Cristo Valley, Qf_1 deposits occur as scattered, deeply eroded ballenas along the eastern flank of the Pilot Mountains and on the east side of the Monte Cristo Valley fault zone (Figs. 3, 7).

Qf_1 soils are durargids containing remnant Bt horizons and well-developed Bqkm horizons.[2] The argillic horizons are commonly truncated, but where preserved they are 15–25 cm thick, reddened (7.5 YR), and strongly prismatic. The Bqkm horizons are strongly indurated (stage IV+ carbonate) and commonly more than 1 m thick.

Unit Qf_2. Late Pleistocene fan-piedmont remnants (Qf_2) displaying well-developed desert pavement and dark rock varnish form a series of broad, flat, interfluvial surfaces inset below the older Qf_1 surfaces. In Monte Cristo Valley, Qf_2 deposits extend eastward from the Pilot Mountains to the Monte Cristo Valley fault zone where they form low-relief, footwall topography in the center of the valley (Figs. 3, 7).

On the basis of inset topographic relationships and soils data, Qf_2 deposits are divided into two subunits. Qf_{2a} deposits contain haplargid and durargid soils exhibiting moderately developed argillic and secondary carbonate horizons. The Bt horizons typically have 20–30-cm-thick, reddened (10YR), medium to strong prismatic, loamy clay soil properties. They overlie 60–100-cm-thick Bkm or Bqkm (stage III–IV) horizons typically containing 10-mm-thick carbonate clast coatings and pendants and 5-mm-thick carbonate-silica laminae. Qf_{2b} deposits are commonly inset 1–2 m below the older Qf_{2a} fan surfaces, and they may be distinguished by their slightly less developed soils. They contain haplargid soils with 15–25-cm-thick loamy clay Bt horizons that are reddened (10YR) and weakly prismatic. The 30–50-cm-thick Bk (stage II–III) horizons are less developed than Qf_{2a} horizons, characteristically exhibiting carbonate coatings and pendants 5–10 mm thick.

Unit Qf_3. Late Pleistocene and Holocene alluvial-fan and wash-terrace deposits (Qf_3) form expansive parts of the mountain drainages and alluvial piedmonts. These deposits lack the well-

[2]Soil horizon terminology is from Soil Survey Staff (1975); carbonate stage terminology from Gile et al. (1966).

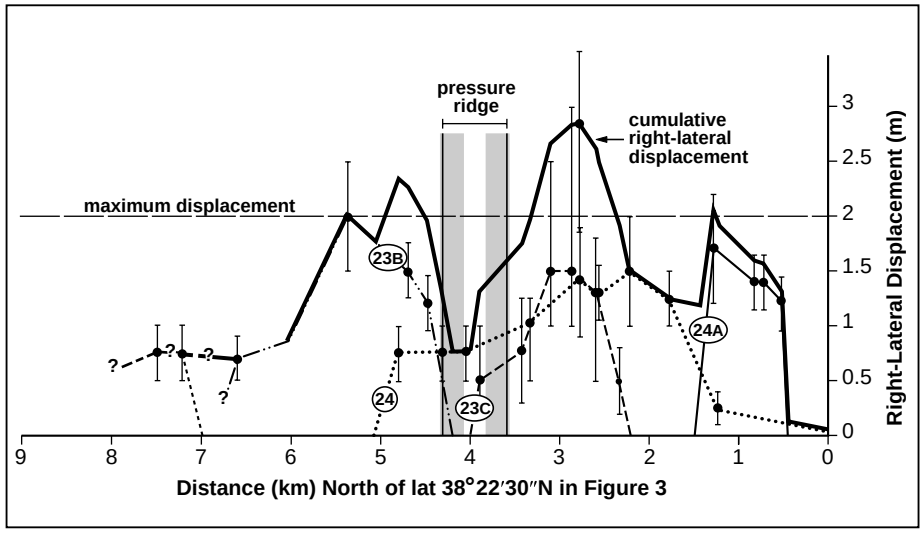

Figure 4. Plot of individual trace and cumulative (bold) 1932 displacements measured across Monte Cristo Valley faults traces 23B, 23C, 24, and 24A. Uncertainty bars indicate range of values measured across individual traces. Maximum displacement line (2 m) represents a mode for individual trace displacements. Small displacements measured in the vicinity of the pressure ridge suggest that strain was likely released predominantly through contractional faulting or folding.

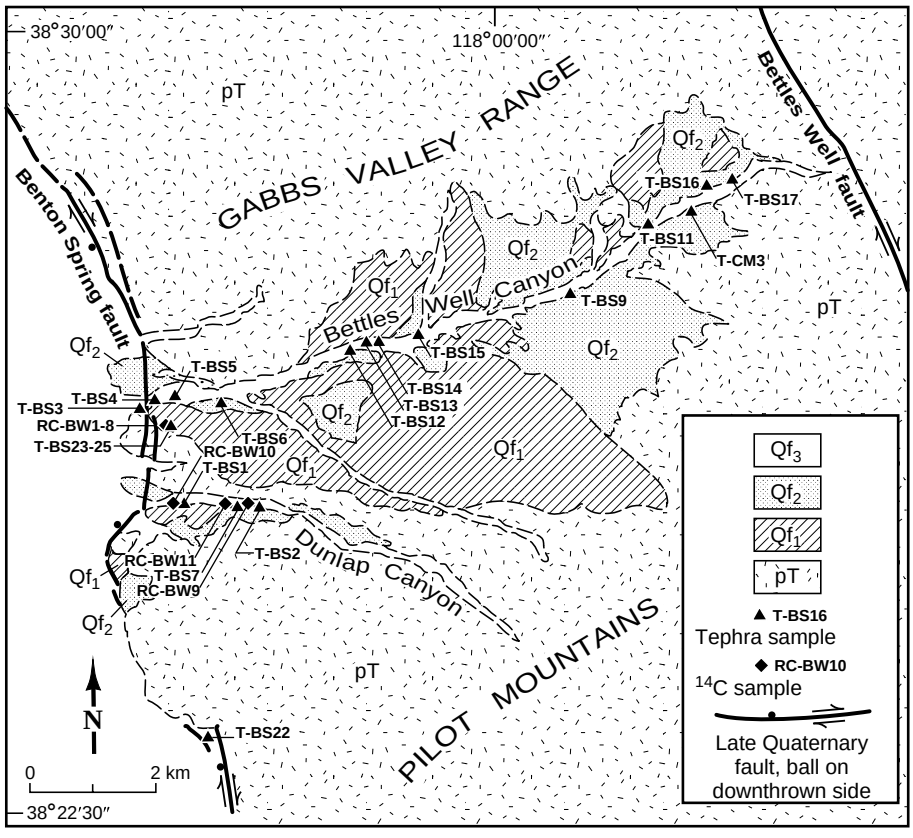

Figure 5. Map of allostratigraphic units in Bettles Well Canyon and location of tephra and radiocarbon sample sites. pT—pre-Tertiary rocks; Qf_1—early and middle Quaternary fan deposits; Qf_2—late Pleistocene fan deposits; Qf_3—late Pleistocene–Holocene fan deposits.

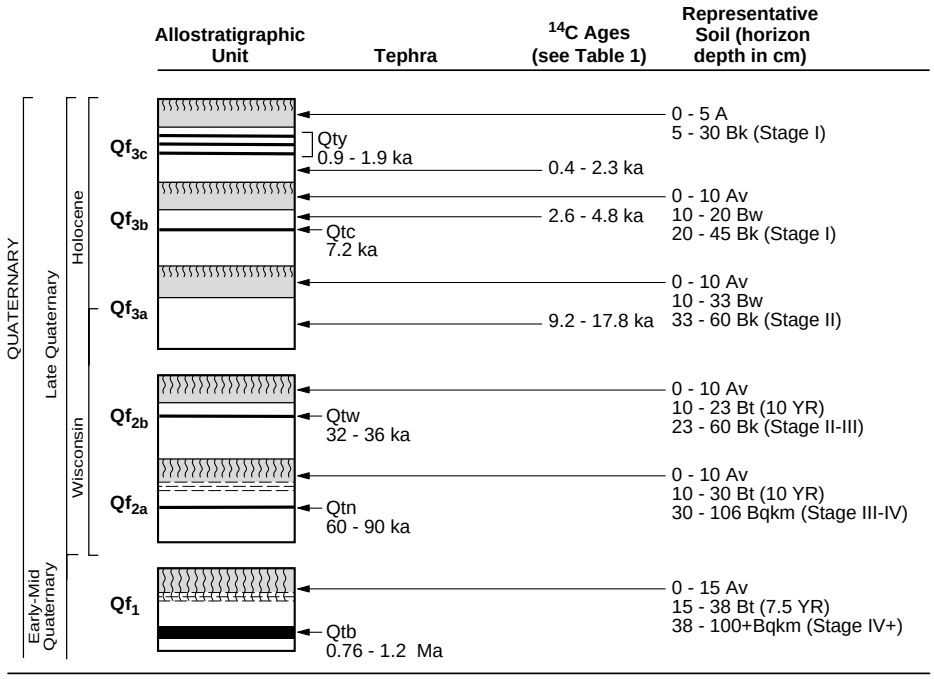

Figure 6. Generalized Quaternary stratigraphic column showing allostratigraphy, tephra, ^{14}C ages, and soil relationships in the Cedar Mountain region. Arrows indicate position of age data within the unit.

developed, tightly packed desert pavement and dark rock varnish that characterize the older Qf_1 and Qf_2 units.

The unit can be divided into early (Qf_{3a}), middle (Qf_{3b}), and late (Qf_{3c}) subunits on the basis of microtopographic, soil, and rock-varnish characteristics. Qf_{3a} has broad, flat interfluvial remnants exhibiting moderately developed, loosely packed desert pavement and moderately dark rock varnish. Soils are camborthids with 20-cm-thick cambic (Bw) horizons and 30-cm-thick stage II calcic (Bk) horizons. Qf_{3b} is characterized by rough to slightly muted bar-and-swale microtopography and weakly developed desert pavement and rock varnish. Soils are camborthids with 10-cm-thick Bw horizons and stage I Bk horizons. Secondary carbonate is present as thin (1 mm) clast coatings and disseminated matrix fillings. Qf_{3c} is similar to Qf_{3b}, but it contains a less-developed (A–C) soil. It forms extensive terraces in most principal drainages and constitutes a large area of the alluvial piedmont in Monte Cristo Valley.

Exploratory Trenching

Exploratory trenches excavated across 1932 ruptures in Monte Cristo Valley yielded key evidence of structural and stratigraphic relationships bearing on the paleoseismic history of the fault zone. Trench 3 is located across the central part of rift 24; trench 6 is located about 1 km north of trench 3 near the left-stepover between rifts 23B and 24 (Figs. 3, 7).

Trench 3. Trench 3, consisting of two parallel trenches 3A and 3B (Fig. 8), is across a fault trace exhibiting 1–2 m of right offset and 30 cm of vertical offset in 1932. Fault geometry is marked by near-vertical to 80°W-dipping flower structure; subhorizontal (plunge 10°N) slickensides and mullions from 1932 and older slip are preserved on carbonate-cemented fault gouge.

Trenches 3A and 3B expose Qf_{2b} and Qf_3 deposits downfaulted against eastward-tilted Qf_1 and Qf_{2b} deposits and Tertiary rocks. Qf_1 deposits in the eastern (footwall) sections contain intercalated volcanic ash (T-CM1); Qf_1 deposits are not exposed in the western (hanging-wall) sections of either trench. Flat-lying Qf_{2b} fan gravel caps the tilted footwall deposits and contains a 50-cm-thick stage II–III Bk soil. In the hanging wall, Qf_{2b} deposits contain a 1-m-thick silt layer.

Four faulted Qf_3 silt layers are differentiated by sedimentologic properties and soils in the hanging-wall sections of both trenches. Subunit Qf_{3a} is a thin (<15 cm) silt layer that lies on eroded Qf_{2b} silt and gravel. A hiatus prior to the deposition of Qf_{3a} is reflected by vesicular A and Bw soil horizons and a prominent stone line along the eroded Qf_{2b} contact. Qf_{3b} is a 1–2-m-thick silt and gravelly silt that is divided into two layers on the basis of sedimentologic properties. The lower one, Qf_{3bl}, is massive silt, and the upper one, Qf_{3bu}, is weakly stratified silt containing platy pedogenic partings, Bw, and stage I Bk horizons. Qf_{3c} is massive, sandy silt containing a weak (A–C) soil.

The throw measured between the top of the Qf_{2b} footwall remnant and the eroded top of Qf_{2b} deposits in the hanging wall (lines A-A′ and B-B′ in Fig. 8) is about 2 m. In trench 3B, a proj0ection of the uneroded Qf_{2b} hanging-wall remnant to the fault scarp yields a vertical throw of about 1 m (line C-C′ in Fig. 8). On the basis of the bounds provided by these three measurements, we estimate the cumulative throw in Qf_{2b} to range between 1 and 2 m.

Trench 6. Trench 6 exposes a thick, well-differentiated sequence of faulted Qf_{2b} and Qf_3 deposits similar to that found in trenches 3A and 3B (Fig. 8). In the eastern footwall, Qf_1 deposits are absent, and Qf_{2b} gravels lie unconformably on highly sheared Tertiary sedimentary rocks.

Five Qf_3 silt layers overlie downfaulted Qf_{2b} gravels in the hanging wall. The lowermost subunit Qf_{3a} is massive silt and gravelly silt lying disconformably on a 10–15-cm-thick A horizon developed in Qf_{2b} gravels. On the basis of the presence of a weak paleosol in the middle of the subunit, Qf_{3a} is further divided into lower and upper layers (Qf_{3al} and Qf_{3au}). The top of Qf_{3au} contains a prominent 10-cm-thick A horizon that forms a sharp contact with a basal stone line in the overlying Qf_{3b} silt subunit. Qf_{3b} deposits are divided, as in trenches 3A and 3B, into two layers. The lower layer (Qf_{3bl}) is massive, gravelly silt; the upper layer (Qf_{3bu}) is weakly bedded silt displaying platy partings and containing a weakly developed (Bw/stage I Bk) soil. At the fault, gravels concentrated both within the basal part of Qf_{3bl} and separating the two Qf_{3b} layers are interpreted as scarp-derived, colluvial-wedge deposits. The uppermost subunit in trench 6 (Qf_{3c}) is a massive sandy silt containing a weak A–C soil. At the west end of the trench, a thin layer of post-1932 silt overlies Qf_{3c}.

Trench 6 crosses the northern end of rift 24 that had an unusually large (50 cm) vertical offset. We attribute this anomalously large displacement to the restraining-bend deformation occurring between rifts 23B and 24. Cumulative throw in Qf_{2b} deposits at trench 6 is 3–4 m (Line D-D′ in Fig. 8), but because the 1932 vertical offset at this site was atypical, we do not consider displacement data from this site in our paleoseismic analysis.

Numerical Age Data

Radiocarbon Dating. Twenty-four conventional and AMS (accelerator mass spectrometer) radiocarbon ages (Table 1) were obtained from deposits exposed in the Monte Cristo Valley trenches (Figs. 3, 8) and from outcrops in Bettles Well Canyon (Fig. 5). Radiocarbon ages obtained from trenches 3A, 3B, and 6 are mean residence time (MRT) ages on buried, weakly organic A horizons. MRT analyses measure the composite, or bulk, ^{14}C content of soil organic materials (humus), and they have been previously used in a variety of pedologic settings to approximately estimate the age of relict and buried soils (Geyh et al., 1971; Orlova and Panychev, 1993; Chichagova and Cherkinsky, 1993). Forman et al. (1989) and Machette et al. (1990) developed the application of MRT soil dating for use in paleoseismic studies.

Tephrochronology. Silicic volcanic tephra layers present in several of the allostratigraphic units provide the principal basis for regional stratigraphic age control (Fig. 6). The layers contain ash-size pyroclastic ejecta derived from the Mono Basin–Long Valley volcanic center of eastern California, about 100 km southwest of the Cedar Mountain area. Major element compositions of the volcanic glass in 17 samples were determined by electron microprobe following sample and analytical procedures described in Sarna-Wojcicki et al. (1984). Tephra samples from the Cedar Mountain area were correlated by glass chemistry with dated tephra layers found in the Mono Basin–Long Valley area and with tephra layers identified in sedimentary cores taken from Walker Lake about 75 km northwest of the Cedar Mountain area (Sarna-Wojcicki et al., 1988). Chemical compositions of sampled tephra layers and comparative compositions of correlative dated tephra layers in the region are available.[3]

The oldest Quaternary tephra layer is Bishop or Glass Mountain ash (0.76 to 1.2 Ma, Sarna-Wojcicki and Pringle, 1992). Tephra sample T-CM1 occurs in Qf_1 deposits at trench 3; this tephra layer is most chemically similar to Glass Mountain "D" and "G" ash beds (0.9 and 1.2 Ma, respectively), but owing to a chemical similarity with Bishop ash (0.76 Ma), it cannot be positively identified without additional data.

All other Quaternary tephra layers identified in the study area were derived from multiple eruptions of the Mono Craters and possibly of Mammoth Mountain in Long Valley (California). We distinguish three sets of Mono Craters and Mono Craters–like ash layers: an older upper Pleistocene set (60–90 ka), a younger upper Pleistocene set (12–36 ka), and a Holocene set (0.5–7.2 ka). The glass compositions of these three sets are all quite similar, and best-fit correlations are made on the basis of similarity coefficients for other known tephra layers in the tephrochronology database at the U.S. Geological Survey in Menlo Park, California.

The oldest upper Pleistocene set of Mono Craters tephra layers (Qtn) occurs in Qf_{2a}, and this set is best correlated with a series of chemically similar beds likely derived from proto–Mono Craters eruptions. At Negit Causeway near Mono Lake (California), these ash beds are intercalated with tephra layers probably derived from Mammoth Mountain. Interstratified tephra beds from the two sources are also found in the Walker Lake cores where they are dated between 60–90 ka (Sarna-Wojcicki et al., 1988).

The younger upper Pleistocene tephra beds (Qtw) occur as thin (2–3 cm) layers in subunit Qf_{2b}, and they are correlated with a series of Mono Craters beds exposed in Wilson Creek at Mono Basin (Benson et al., 1990). The closest matches for samples T-BS6 and T-BS17 (Fig. 5) are the Wilson Creek beds 16 through 19, radiocarbon dated at 32–36 ka. There are, however, a number of other possible matches with tephra layers that are older and deeper in the Walker Lake cores.

Holocene ash eruptions from Mono Craters covered more than 8000 km^2 of eastern California and western Nevada (Wood, 1977; Sieh and

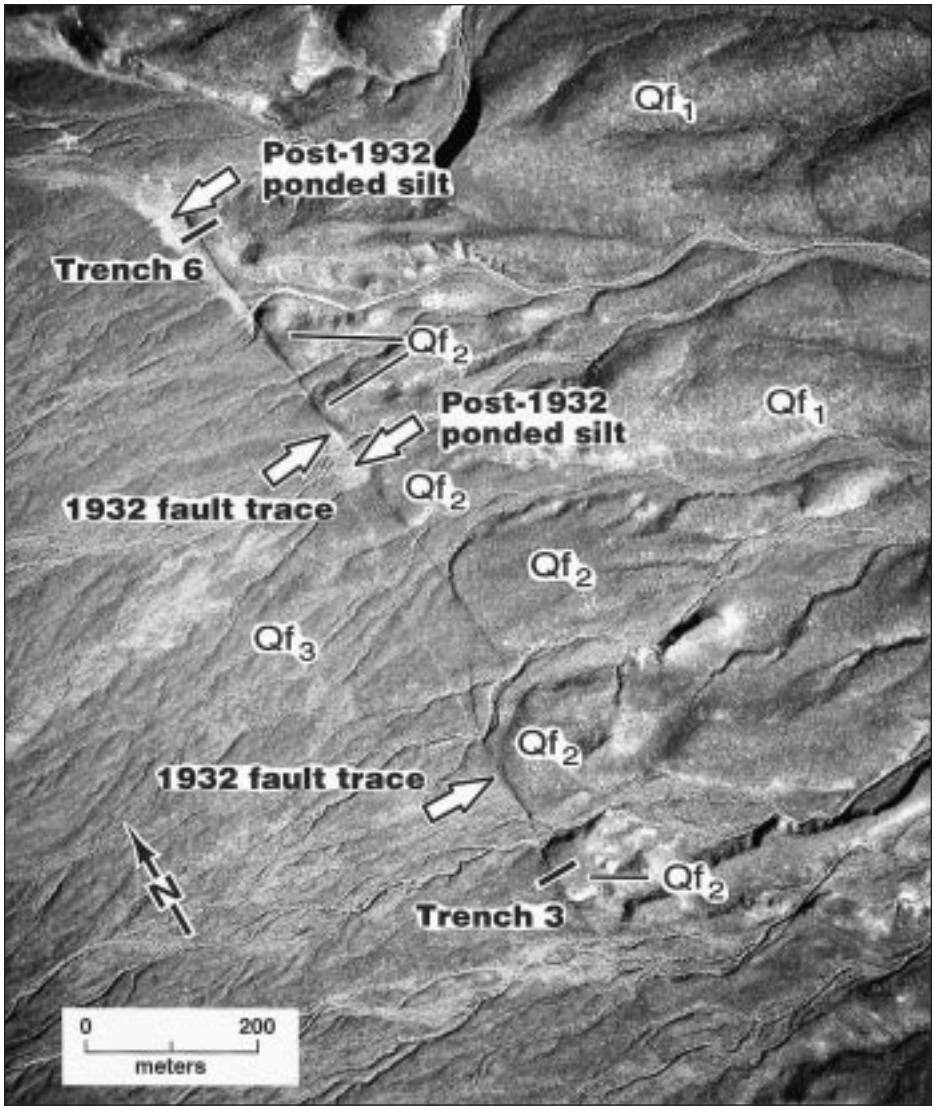

Figure 7. Low–sun-angle aerial photograph of rift 24 showing 1932 fault trace, trench locations, surficial deposits, and areas of silt ponded against 1932 fault scarps. (Photograph CMT-HF-1-125, flown January 18, 1968; from the collection of D. B. Slemmons.)

[3]GSA Data Repository item 9949, supplemental data table, is available on request from Documents Secretary, GSA, P.O. Box 9140, Boulder, CO 80301. E-mail: editing@geosociety.org. Web: http://www.geosociety.org/pubs/ftpyrs.htm.

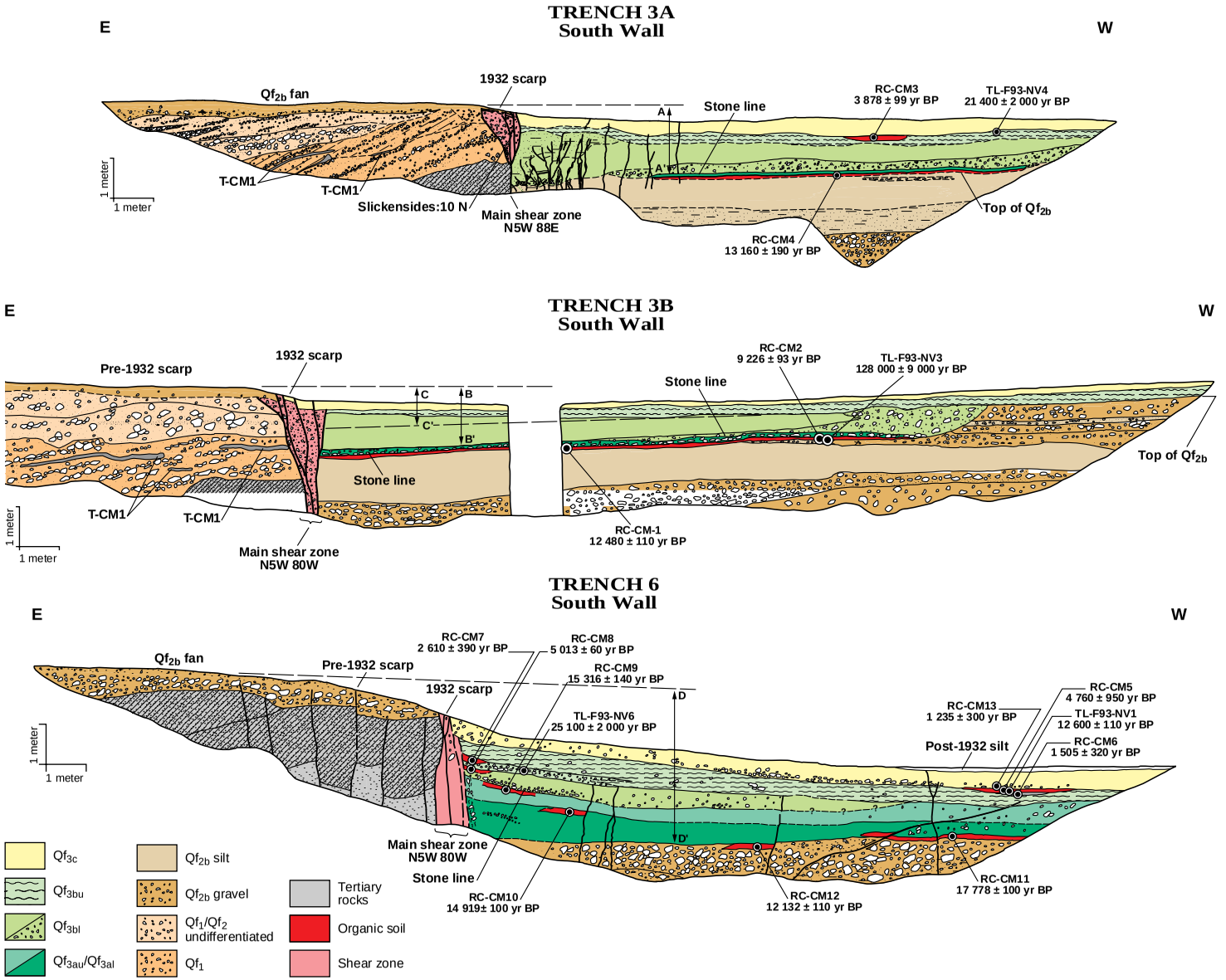

Figure 8. Diagrams (logs) of deposits exposed in exploratory trenches 3A, 3B, and 6 located across rift 24 in Monte Cristo Valley (see Fig. 3). The eastern footwall sections of the trenches are composed of middle to late Pleistocene alluvial-fan (Qf_1, Qf_2) deposits overlying Tertiary sedimentary rocks. The T-CM1 bed in Qf_1 deposits is Bishop–Glass Mountain ash (0.76–1.2 Ma); the offset Qf_{2b} deposits contain a 32–36 ka Mono Craters tephra in adjacent areas. The western hanging-wall sections are composed of stacks of silt beds (Qf_{2b} silt, Qf_{3a}, Qf_{3b}, and Qf_{3c}) overlying downthrown late Pleistocene alluvial-fan (Qf_{2b}) deposits. The silt beds are each interpreted to represent an earlier faulting event, and each bed is separated by a weakly organic soil (shown in red) that has been dated by mean-residence-time (MRT) radiocarbon analysis. The locations and ages of radiocarbon (RC) and thermoluminescence (TL) samples are indicated and further described in Tables 1 and 2. Lines A–A′, B–B′, C–C′, and D–D′ indicate separately determined estimates of cumulative vertical throw in Qf_{2b} deposits during the last 32–36 ka. A synthesis of the MRT ages and interpretation of the timing of five pre-1932 fault events are shown in Figure 9.

TABLE 1. RADIOCARBON DATING RESULTS

Sample	Material dated	^{14}C yr (lab #)	Calibrated yr* (±1σ)	Location
RC-1	Wood	235 ± 65 (GX-13952)	289^{+20}_{0}	Unfaulted subunit Qf_{3c} alluvium predating 1932 faulting
RC-BW4	Peat	435 ± 110 (GX-17253)	503^{+47}_{-153}	30 cm above tephra T-BS25
RC-BW2	Peat	535 ± 150 (GX-17251)	547^{+123}_{-77}	6 cm above tephra T-BS23
RC-BW5	Peat	790 ± 105 (GX-17254)	706^{+94}_{-36}	6 cm above tephra T-BS25
RC-BW1	Woody peat	995 ± 110 (GX-17250)	935^{+145}_{-65}	6 cm above tephra T-BS23
RC-BW6	Peat	1025 ± 65 (GX-17255)	950^{+40}_{-35}	6 cm below tephra T-BS25
RC-BW7	Woody peat	1110 ± 110 (GX-17256)	1008^{+152}_{-68}	6 cm above tephra T-BS24
RC-CM13	Soil organic material	1 235 ± 300 (GX-20334)	1175^{+295}_{-245}	Trench 6; base of subunit Qf_{3c}
RC-BW3	Woody peat	1260 ± 145 (GX-17252)	1199^{+111}_{-189}	Disturbed zone above tephra T-BS25
RC-BW10	Soil organic material	1505 ± 200 (GX-18939)	1388^{+222}_{-128}	3 cm above tephra T-BS1
RC-CM6	Soil organic material	1505 ± 320 (GX20327)	1388^{+290}_{-372}	Trench 6; buried Av horizon in silt layer Qf_{3bu}
RC-BW8	Peat/charcoal	1550 ± 110 (GX-17257)	1433^{+127}_{-103}	8 cm below tephra T-BS24
RC-BW9	Charcoal	1605 ± 120 (GX-17566)	1522^{+108}_{-152}	Immediately above tephra T-BS2
RC-BW11	Soil organic material	2355 ± 405 (GX-18940)	2361^{+498}_{-461}	Buried Av horizon immediately below tephra T-BS2; T-BS7
RC-CM7	Soil organic material	2610 ± 390 (GX-20328)	2757^{+458}_{-390}	Trench 6; buried Av horizon at top of colluvial wedge in silt layer Qf_{3bu}
RC-CM3	Soil organic material	3878 ± 99 (GX-16785)†	4337^{+174}_{-109}	Trench 3; buried Av horizon at top of platy silt layer Qf_{3bu}
RC-CM5	Soil organic material	4760 ± 950 (GX-18938)	5491^{+1262}_{-1018}	Trench 6; buried Av horizon at top of platy silt layer Qf_{3bu}
RC-CM8	Soil organic material	5013 ± 60 (GX-20329)†	5755^{+73}_{-133}	Trench 6; buried Av horizon at top of silt layer Qf_{3bl} and beneath colluvial wedge in silt layer Qf_{3bu}
RC-CM2	Soil organic material	9226 ± 93 (GX-16784)†	$10\,171^{+153}_{-118}$	Trench 3; buried Av horizon at top of silt layer Qf_{3au} and beneath prominent stone line
RC-CM12	Soil organic material	12132 ± 110 (GX-20333)†	$14\,157^{+153}_{-145}$	Trench 6; buried Av horizon at top of subunit Qf_{2b} gravel and beneath silt layer Qf_{3a}
RC-CM1	Soil organic material	12480 ± 110 (GX-16783)†	$14\,621^{+173}_{-166}$	Trench 3; buried Av horizon at top of silt layer Qf_{3au} and beneath prominent stone line
RC-CM4	Soil organic material	13160 ± 190 (GX-16786)†	$15\,683^{+279}_{-304}$	Trench 3; buried Av horizon at top of silt layer Qf_{3au} and beneath prominent stone line
RC-CM10	Soil organic material	14919 ± 100 (GX-20331)†	$17\,832^{+114}_{-112}$	Trench 6; buried Av horizon at top of silt layer Qf_{3al}
RC-CM9	Soil organic material	15316 ± 140 (GX-20330)†	$18\,237^{+138}_{-142}$	Trench 6; buried Av horizon at top of silt layer Qf_{3au} and beneath prominent stone line
RC-CM11	Soil organic material	17778 ± 110 (GX-20332)†	$21\,195^{+164}_{-164}$	Trench 6; buried Av horizon at top of subunit Qf_{2b} gravel and beneath silt layer Qf_{3al}

Note: Bulk soil preparation and analyses by Geochron Laboratories, Cambridge, Massachusetts.
*Calibrated from Stuiver and Reimer (1993).
†Accelerator (AMS) date.

Bursik, 1986). In the Cedar Mountain region, these tephra beds are ubiquitous, thin (1–2 cm) beds in Qf_{3b} and Qf_{3c} deposits. Tephra layer Qtc (sample T-BS9; Fig. 5) is a moderately hydrated ash best matched with a middle Holocene (7.2 ka) tephra bed found at Crooked Meadow (California) (K. R. Lajoie and A. M. Sarna-Wojcicki, unpublished data). The upper Holocene tephra layers (Qty) are variously correlated with chemically similar beds found in Walker Lake, Mono Lake, and Barrett Lake (California) and with exposures in the Mono-Panum Crater area. These tephra layers range in age from 890 to 1950 yr B.P. Tephra T-BS2 is bracketed by ^{14}C ages of 1605 ± 120 yr B.P. (RC-BW9, Table 1) and 2355 ± 405 yr B.P. (RC-BW11) in Dunlap Canyon (Fig. 5). At the mouth of Bettles Well Canyon, several tephra beds (T-BS23–T-BS25), which were not chemically analyzed but are petrographically similar to the microprobe samples, are interstratified with peat deposits ^{14}C dated between 435 ± 110 yr B.P. (RC-BW4) and 1550 ± 110 yr B.P. (RC-BW8). At Walker Lake, these tephra beds are contained within organic sediments dated between 0.4 and 4 ka (Sarna-Wojcicki et al., 1988).

Thermoluminescence Dating. Thermoluminescence (TL) dating can provide numerical ages for buried sedimentary deposits younger than ca. 100 ka (Wintle and Huntley, 1982). The technique estimates the time elapsed since the TL signature in the sedimentary mineral grains was reset by bleaching in sunlight. In this study, TL analyses were performed on four samples taken from trenches 3 and 6 (Fig. 8, Table 2). Samples were collected from the A horizon in subunit Qf_{3a} in trench 3A, from the small colluvial wedge in Qf_{3bu} in trench 6, and from the A horizons capping Qf_{3bu} in trenches 3A and 6. The samples were analyzed by using the partial- and total-bleach laboratory procedures described in Forman (1989).

Evaluation of Dating Results

Results from the multiple dating techniques were evaluated by considering uncertainties associated with each methodology and examining stratigraphic consistencies.

TABLE 2. THERMOLUMINESCENCE DATA AND AGE ESTIMATES FOR SAMPLES COLLECTED FROM MONTE CRISTO VALLEY TRENCHES

Field number	Lab sample number	Stratigraphic unit	Equivalent dose method*	Light exposure†	Temperature (°C)§	Equivalent dose (Gy)	TL age Est. (ka)#
TL-F93-NV1	OTL426	top Qf_{3bu}	TL–total bleach	16 h sun	300–400	63.4 ± 3.6	12.6 ± 1.1
			TL–part bleach	1 h	300–400	58.2 ± 3.4	10.6 ± 1.0
TL-F93-NV3	OTL427	top Qf_{2b}	TL–total bleach	16 h sun	250–400	570.8 ± 10.1	128 ± 9*
TL-F93-NV4	OTL433	top Qf_{3bu}	TL–total bleach	16 h sun	250–400	78.3 ± 4.9	21.4 ± 2.0
			TL–part bleach	1 h	280–310	92.5 ± 9.7	25.3 ± 2.9**
TL-F93-NV6	OTL432	top Qf_{3bl}	TL–total bleach	16 h sun	270–400	100.9 ± 3.1	25.1 ± 2.0

Note: Analyses by S. L. Forman, Ohio State University (present address: University of Illinois, Chicago campus).
*All TL measurements were made with a 5-58 filter (blue wavelengths) and HA-3 filters in front of the photomultiplier tube. Samples were preheated to 1240 °C for 2 days prior to analysis.
†Hours or minutes of light exposure to define residual level. "Sun" is natural sunlight in Columbus, Ohio.
§Temperature range used to calculate equivalent dose.
#All errors are at 1σ and calculated by averaging the errors across the temperature range.
**Problematic analysis; sample rejected.

Previous work suggests that MRT ages may display a range of uncertainty of 1000 yr or more owing to recycled, older carbon present in a soil at the time of burial and/or the postburial addition of young carbon through bioturbation and root activity (Chichagova and Cherkinsky, 1993). We do not know precisely how much uncertainty is associated with each age in this study, but we compared our MRT ages for both internal consistency and for agreement with other independent ages.

Of the 13 MRT ages obtained from trenches, 10 are in consistent stratigraphic order (Fig. 8; Table 1). Three ages are not stratigraphically consistent: Sample RC-CM12 (12 132 ± 110 yr B.P.) is anomalously young by 3000–5000 yr compared to overlying samples RC-CM9, RC-CM10, and RC-CM11. Consequently, we have not considered the age of this sample in our paleoseismic interpretations. The ages of RC-CM9 (15 316 ± 140 yr B.P.) and RC-CM10 (14 919 ± 100 yr B.P.) are inverted as are the ages of RC-CM7 (2610 ± 390 yr B.P.) and RC-CM5 (4760 ± 950 yr B.P.), but the inversions are within the range of uncertainties (±1000 yr) associated with MRT dating.

The closely similar glass chemistries used to correlate some tephra beds are the principal sources of uncertainty associated with the assigned tephra ages. Most of the tephra beds occur within units dated by other stratigraphic and numerical dating means, providing confirmation of tephra correlations.

The four TL total-bleach ages (Table 2) are inconsistent with trench stratigraphy, and they are older by factors of two to five than the MRT ages obtained from the same units. The TL age obtained from subunit Qf_{3a} in trench 3B (128 ± 9 ka, TL-F93-NV3) was rejected on the basis of a problematic laboratory analysis. The 25.1 ± 2.0 ka age from TL-F93-NV6 in trench 6 layer Qf_{3bl} is unsupported by any of the MRT ages. Conflicting TL ages of 21.4 ± 2.0 ka (TL-F93-NV4) and 12.6 ± 1.1 ka (TL-F93-NV1) were obtained from correlative Qf_{3bu} layers in trenches 3A and 6, and this horizon was MRT dated at between 1.2 ± 0.3 and 4.8 ± 0.9 ka (Fig. 8). We do not know why there are such large discrepancies between the TL and other age data, but possible reasons may include insufficient resetting by sunlight and inheritance of a prior TL signature. On the basis of these inconsistencies, we do not consider the TL ages in the paleoseismic analysis.

Integration of Stratigraphic and Numerical Age Data

Unit Qf_1 is middle Quaternary in age on the basis of the presence of Bishop–Glass Mountain "G" ash (Qtb, 0.76–1.2 Ma). The unit contains several undifferentiated subunits defined by inset topographic relationships, and it is likely that this ash provides only an approximate age for the composite unit.

The two subunits of Qf_2 are dated by tephra layers as late Pleistocene in age. Subunit Qf_{2a} contains proto–Mono Craters and Mammoth Mountain tephra beds (Qtn) having an age range of 60–90 ka, placing the deposit in the early Wisconsinan pluvial period. Subunit Qf_{2b} forms an important alluvial-geomorphic datum for interpreting the paleoseismic history of the Cedar Mountain region, and a maximum age for the unit is established by the 32–36 ka Qtw tephra layer. The age of the tephra bed places the unit in the late Wisconsinan pluvial period and indicates that it is likely correlative with other late glacial-pluvial deposits of the western Basin and Range region (cf. Peterson et al., 1995).

Numerical age control is provided for unit Qf_3 by tephra layers and radiocarbon ages of buried organic material. Subunit Qf_{3a} is placed in the late Pleistocene to early Holocene by multiple MRT ages obtained from trenches 3 and 6. Six MRT ages range from 9.2 ± 0.9 to 15.3 ± 0.1 ka (RC-CM1, RC-CM2, RC-CM4, RC-CM9, RC-CM10, RC-CM12, Table 1). The age of Qf_{3a} is estimated to be 8–16 ka, with a maximum age provided by the 17 778 ± 110 yr B.P. date (RC-CM11) on the soil immediately underlying Qf_{3al} in trench 6. Subunit Qf_{3b} contains the 7.2 ka tephra Qtc. An MRT age of 3.9 ± 1.0 ka was obtained from the upper part of Qf_{3b} in trench 3A. We estimate an age range of 4–8 ka for Qf_{3b}. A late Holocene age of 0.9 to 1.9 ka is indicated for Qf_{3c} by multiple Qty tephra beds. Organic material from Qf_{3c} deposits in Bettles Well Canyon yielded 11 conventional ^{14}C ages between 435 ± 110 (RC-BW4, Table 1) and 2355 ± 405 yr B.P. (RC-BW11). MRT ages of 1.2 ± 0.3 and 1.5 ± 0.3 ka were obtained from the soil underlying Qf_{3c} in trench 6 (RC-CM13, RC-CM6). On the basis of these data, we estimate the age of Qf_{3c} to be <2.5 ka.

DISCUSSION

Paleoseismic History

Monte Cristo Valley. The most relevant paleoseismic data come from Monte Cristo Valley where primary surface rupturing occurred along late Quaternary faults (Fig. 3). Faulting in Stewart Valley cannot be associated with any visible paleoseismic features. On the basis of the north-striking strike-slip focal mechanism for the

main event, we conclude that the small, north-northeast–striking normal faulting in Gabbs Valley was either secondary or sympathetic, despite being located closer to the main epicenter.

Units Qf_2 and Qf_3 provide broad constraints on locations and rates of late Quaternary fault activity in Monte Cristo Valley where they form the bulk of the alluvial piedmont sloping eastward from the Pilot Mountains to the valley floor (Fig. 3). The Monte Cristo Valley fault zone has displaced this eastward-sloping piedmont down to the west, creating upraised, back-facing topography. West-facing 1932 scarps blocked principal drainages, resulting in localized ponding of stream sediment. Best displayed north of trench 6 (Fig. 7), as much as 50 cm of post-1932 silt was deposited along the scarp.

Although Qf_2 and Qf_3 deposits straddle both sides of the Monte Cristo Valley fault zone, little long-term geomorphic evidence of lateral offset, such as offset stream channels, is visible in these units. We believe that the lack of such evidence is due to a combination of long recurrence intervals, extensive piedmont alluviation during the Holocene, rapid regrading of offset channel gradients, and ponding of sediment against the scarps.

Interpretation of Trenches 3 and 6. The stacks of silt layers the age of Qf_3 that are exposed in the hanging walls of trenches 3 and 6 are interpreted to be tectonically ponded fluvial sediments analogous to those impounded by 1932 faulting. The similar thickness and sedimentologic character of each silt layer, particularly in trench 6, suggest that the scarps were effective sedimentary traps that could not be bypassed by the drainages.

The degradation of fault scarps formed in gravelly alluvium is commonly reflected by poorly sorted, wedge-shaped colluvial deposits on the hanging wall. The ponded silts are not colluvial-wedge deposits because they were not produced by scarp erosion, but they are similar in that deposition occurred in response to fault displacement. Although the trenches lack distinctive colluvial wedges, the gravel concentrations in trench 6 Qf_{3b} deposits and the thickening of some deposits near the fault suggest that there has been some contribution of colluvium from the scarp.

The lack of distinctive colluvial wedges is supportive of small vertical offsets, such as in 1932, because small scarps can produce only minor colluvial debris. Alternatively, we cannot completely preclude the possibility that the silt deposits are in part related to pulses of fan deposition rather than to faulting.

The silts were deposited since 17.8 ± 0.1 ka on the basis of the age of RC-CM11 beneath Qf_{3al} (Fig. 8). In addition, the paleosols developed in the silts support a late Pleistocene–Holocene age for the sequence. The weak cambic soils found in the each of the five silt subunits (Qf_{2a}, Qf_{2b}, Qf_{3a}, Qf_{3b}, and Qf_{3c}) are indicative of subaerial weathering intervals individually less than a few thousand years in length (cf. Gile, 1975). Cumulatively, these five soils suggest that the age of the entire sequence is less than ca. 15 ka.

Late Quaternary Slip History in Monte Cristo Valley

If the ponded silt layers found in trenches 3 and 6 are each related to a faulting event, as we believe the evidence suggests, six events including the one in 1932 occurred since deposition of subunit Qf_{2b}. Figure 9A illustrates the relationship between faulting events and dated soils. If silt deposition is assumed to occur in response to faulting, the radiometric age of a buried A horizon should approximate the age of the overlying faulting event (Forman et al., 1989; Machette et al., 1990).

On the basis of the range and inversion of some MRT ages, we interpret approximate, best-fit, fault-event ages with inferred ±2000 yr error bars to account for dating uncertainties. Of the five pre-1932 events, the two earliest faulting events (U and V) are represented by layers Qf_{3al} and Qf_{3au} in trench 6; at trench 3, subunit Qf_{3a} is thin, and these subunits cannot be differentiated (Fig. 8). An age of 18 ka for event U is provided in trench 6 where layer Qf_{3al} lies on the buried soil dated at 17 778 ± 110 yr B.P. (RC-CM11, Table 1). The age of event V is estimated at 15 ka from the 14 919 ± 100 yr B.P. (RC-CM10) date on the soil that is weakly developed in layer Qf_{3al}. The age of event W is estimated to be 12 ka, which is the mean of the four MRT ages from the soil at the top of layer Qf_{3au} (RC-CM1, RC-CM2, RC-CM4, RC-CM9). The timing of event X is estimated at 5 ka on the basis of the 5013 ± 600 yr B.P. (RC-CM8) date from the soil in Qf_{3bl}. Event Y is dated by four MRT ages from layer $Qf_{3bu,}$ which range from 1.5 to 4.8 ka (RC-CM3, RC-CM5, RC-CM6, RC-CM7). We believe that the relatively comparable ages of 3878 ± 990 and 4760 ± 500 yr B.P. from trenches 3A and 6 suggest that the soil is close to the older end of this range, and we infer a best-fit age of 4 ka for event Y.

On the basis of a maximum age of 32–36 ka for faulted Qf_{2b} deposits, the occurrence of six events since the deposition of Qf_{2b} indicates an average recurrence interval of between 5 and 6 ka. However, average recurrence can be more precisely determined from the interseismic intervals separating dated events. The age of the soil buried by layer Qf_{3al} in trench 6 suggests that the six events occurred since ca. 17.8 ka (sample RC-CM11). The average of the five interseismic intervals occurring between event U and 1932 is 3600 yr. Alternatively, if the silts are related to nontectonic pulses of fan deposition, there could be fewer events with longer recurrence intervals even though the long-term slip rate would remain unchanged.

Long-term slip rates are best estimated at trench 3 where 1932 and older displacements are judged to be more typical than at trench 6. Trench 3 measurements show 1 to 2 m of right-lateral displacement and 30 cm of vertical displacement for the 1932 earthquake. This ratio of horizontal-to-vertical slip agrees with the 6:1 ratio indicated by the 10°N-plunging slickensides found on carbonate-cemented fault gouge. On the basis of 1–2 m vertical offset of Qf_{2b} deposits, the total amount of right slip (approximately equal to net slip) during the late Quaternary is estimated to be 6–12 m.

The late Quaternary slip rate is determined from offset Qf_{2b} deposits. The maximum age of 32–36 ka for Qf_{2b} deposits and the estimated cumulative net slip of 6–12 m yield an average minimum slip rate of 0.2–0.4 mm/yr. If the age of faulted Qf_{2b} deposits is closer to the 17.8 ka age of the buried soil in trench 6, however, the slip rate could be as much as 0.7 mm/yr. Because the age of the faulted fan surface is necessarily younger than the buried tephra and because the MRT age of the soil is a minimum, the actual slip rate probably lies between 0.2 and 0.7 mm/yr; we prefer a rate of 0.4–0.5 mm/yr.

Evidence for Characteristic Events

Repeated, similar-size displacements on the same fault are suggestive of "characteristic" earthquake behavior (cf. Schwartz and Coppersmith, 1984). Although we cannot determine whether the entire 1932 Cedar Mountain rupture pattern has been characteristically repeated, the apparent repetition of similar-size events in Monte Cristo Valley is suggestive of characteristic slip. Each of the ponded silt layers in trench 6 is similar in thickness to the vertical displacement that occurred at the site in 1932. At trench 3, six events each having 30 cm of vertical offset would account for the observed 1–2 m of cumulative throw measured across faulted Qf_{2b} deposits. Similarly at trench 6, six events each having 50–75 cm of vertical offset would account for the estimated 3–4 m of throw across Qf_{2b} deposits. Alternatively, if fewer but larger vertical displacements occurred, they would indicate greater components of normal slip and/or larger magnitude ($M_s > 7.2$) events on the basis of magnitude vs. displacement relationships (Wells and Coppersmith, 1994).

Evidence for Temporal Clustering

Temporal clustering—the grouping of several seismic events closely in time—may characterize the late Quaternary slip history of some faults in the Basin and Range province (Wallace, 1987).

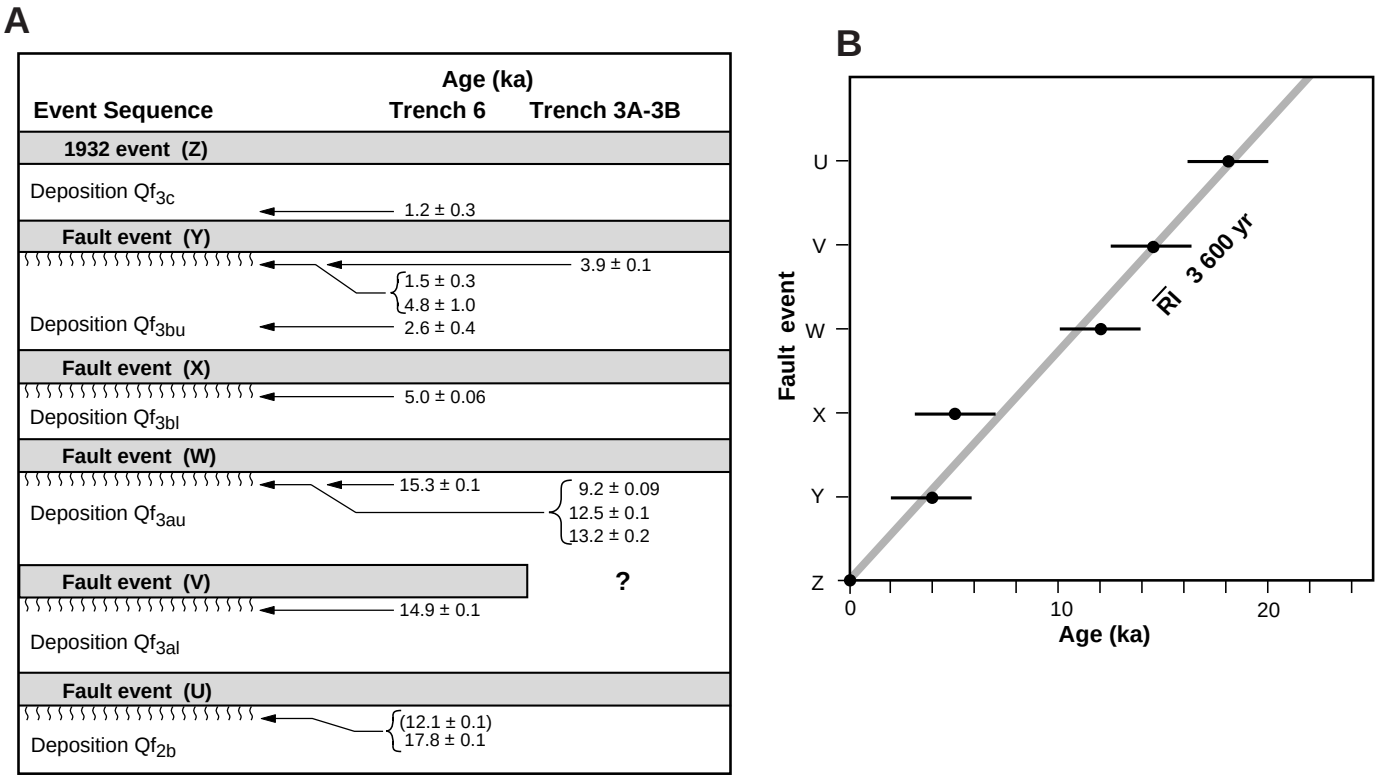

Figure 9. (A) Earthquake event sequence interpreted from trenching results. Six surface-faulting events are placed at the disconformities between each of the ponded silt units and the underlying mean resistence time (MRT) dated paleosols. MRT ages (Table 1) are positioned stratigraphically in the sequence, and arrows indicate correlation with event stratigraphy. Event V is recognized only in trench 6 and cannot be differentiated in trench 3. The anomalously young 12.1 ± 0.1 ka age from below event U is not considered in the dating of events. (B) Time-dependent plot of earthquake event vs. age for each of the six surface-faulting events and comparison with average late Quaternary recurrence interval of 3600 yr. Solid circles indicate the best-fit, interpreted age for each event; ±2000 yr bars account for the estimated uncertainties associated with ranges in MRT soil ages.

Pearthree (1990) used evidence based on fault scarp morphology to conclude that pulses of fault activity had occurred in central Nevada during several episodes in the middle to late Holocene.

In Monte Cristo Valley, however, the resolution of event timing is insufficient to convincingly discriminate temporal clusters. A time-dependent plot of the five pre-1932 events (Fig. 9B) shows that most events lie on or close to the 3600 yr recurrence line, a relationship suggestive of periodic behavior. The principal evidence for aperiodic or clustered activity is related to the age of Qf_{2b} and to the timing of event X. If the actual age of faulted Qf_{2b} deposits is substantially greater than about 24 ka (the age of event U plus one additional interseismic interval), the six events would seem to be clustered within the past 18 ka. Event X appears to be an outlier on the 3600 yr recurrence line. If the 5.0 ± 0.6 ka (RCCM8) age on the Qf_{3bl} soil is an accurate upper limit for event X, then the last three faulting events are separated by two interseismic intervals of about 2500 yr, a value somewhat shorter than the longer-term average.

FAULT MODELS

Previous Models

Several strike-slip fault models have been applied to the distribution and style of faulting that occurred in 1932. Gianella and Callaghan (1934b) attributed the 1932 rupture pattern to a single-event wrench-fault model. Without identifying a causative fault, they proposed that a regional-scale, right-lateral southeastward shift of the Paradise Range–Cedar Mountain block relative to the Gabbs Valley–Pilot Mountain block (Fig. 1B) produced the north-trending, en echelon set of 1932 ruptures. Molinari (1984) later suggested that the 1932 faults were Riedel shears (Riedel, 1929) developed over a concealed, northwest-striking master fault, the Stewart–Monte Cristo Valley fault (Fig. 10, A and B). Doser (1988) proposed a two-event model and located a second subevent near the Petrified Spring fault (CM2, Figs. 1B, 10A, 10B).

Alternative Models

Seismic moment (M_o) is an empirical value that measures the energy released by an earthquake, and it can be estimated from both geologic and seismologic data. Geologic moment is estimated from the relationship

$$M_o = \mu AD,$$

where μ is the shear modulus, A is the area of the fault rupture plane, and D is the average displacement (Brune, 1968).

Instrumental seismic moment (M_o) is measured directly from seismograms, and it is commonly used to calculate the moment magnitude (M_w) of the earthquake. In theory, the independently determined geologic and instrumental

moments should be comparable. However, the geologic moment of 5.4×10^{26} dyne · cm calculated from the 1932 rupture-zone length and average displacement (Table 3, single-event model) is two to three times larger than the instrumental moment of 1.97×10^{26} dyne · cm (two-event model).

Doser (1988) first noted this disparity between the geologic and instrumental seismic moments and suggested that the mismatch may be due to additional subevents masked by the seismic coda. Here, we propose that two alternative fault models that include additional subevents could account for the moment disparity and also explain complexities of the 1932 surface-rupture pattern. In these alternative models, we assume that the CM 2 subevent of Doser (1988) was closer to the main CM 1 epicenter in Gabbs Valley (Fig. 10, A and B) on the basis of the lack of surface faulting on the Petrified Spring fault and the large east-west location errors given for CM 2. Seismogenic slip on either one large north-striking fault or two smaller, closely spaced faults concealed under Gabbs Valley would similarly produce the instrumentally determined moment reported for CM 1 and CM 2.

The primary surface faulting in Monte Cristo Valley strongly suggests that one or more additional subevents occurred in the southern half of the rupture zone. In one alternative model (Fig. 10B), a third right-lateral subevent (CM 3) is hypothesized on a concealed northwest-striking fault beneath Stewart and Monte Cristo Valleys (the Stewart–Monte Cristo Valley [SMC] fault of Molinari, 1984). A second alternative model (Fig. 10C) hypothesizes third and fourth subevents (CM 3 and CM 4) on separate north-striking faults beneath Stewart and Monte Cristo Valleys.

The late Cenozoic pattern of pervasive en echelon strike-slip faulting with components of reverse and extensional slip is generally consistent with wrench-fault kinematics (Moody and Hill, 1956) and Riedel right-lateral simple-shear relationships (Riedel, 1929; Tchalenko, 1970; Wilcox et al., 1973; Naylor et al., 1986; Sylvester, 1988). Some other historical surface-faulting patterns have been explained by similar relationships (Tchalenko and Ambraseys, 1970). In Figure 10D, a strain ellipse illustrating the primary wrench-fault orientation and the corresponding Riedel shear relationships is oriented in the contemporary stress field estimated for the central Nevada region (σ_3 = N53°W; Savage et al., 1995).

In the three-event model, the primary wrench (Stewart–Monte Cristo Valley) fault parallels the traces of the principal transcurrent faults and fits the regional pattern of northwest-striking, left-stepping faults. Right-slip motion on a 30-km-long Stewart–Monte Cristo Valley fault would produce surface rupture in Stewart and Monte Cristo Valleys on the basis of Riedel shear relationships: the north-striking, right-lateral 1932 surface ruptures would correspond to synthetic Riedel (first-order) shears. On a regional scale, the left-lateral faulting associated with the 1934 Excelsior Mountain earthquake would be consistent with the orientation of conjugate Riedel (second-order) shears.

Alternatively, the two north-striking subevents of the four-event model would fit the pattern of observed surface faulting in Monte Cristo Valley and closely correspond to the Doser (1988) focal mechanisms. In this model, the Stewart and Monte Cristo Valley rupture zones would mark the surface traces of two subsurface right-lateral faults, each about 17 km long. Together with the Gabbs Valley fault(s) they would collectively form a left-stepping, en echelon set, and the north-striking subsurface faults would correspond to first-order Riedel shears synthetic to the larger northwest-striking Walker Lane faults.

CONCLUSIONS AND IMPLICATIONS FOR WALKER LANE TECTONICS

The results of surface faulting and paleoseismic studies in the 1932 Cedar Mountain earthquake area allow several conclusions to be drawn bearing on the modern tectonics and earthquake hazards of the Walker Lane region. In contrast to most other historical faults in the Basin and Range province, the Cedar Mountain faulting lacks any obvious structural relationship to a single, throughgoing basement fault, and it is unusual in that it did not occur along a major range-bounding structure. In Monte Cristo Valley, primary right-lateral ruptures occurred along a left-stepping series of low-relief, midvalley faults more than 50 km from the main epicenter. In Stewart Valley, surface deformation cannot be associated with any principal fault and may be related to folding in the Tertiary-Quaternary sedimentary section. In Gabbs Valley, secondary or sympathetic normal faulting occurred on more than a dozen separate faults scattered throughout the valley.

On the basis of these spatial and structural relationships, we believe that the 1932 Cedar Mountain earthquake is perhaps the best example from among several historical Basin and Range province earthquakes to illustrate how distributive surface faulting may accompany large-magnitude events. The 1932 and other large seismic events—such as the 1992 Landers, California (Johnson et al., 1994), and 1954 Fairview Peak (Slemmons, 1957), Nevada, earthquakes—support the concept that major earthquakes in the Basin and Range province can exhibit complicated rupture patterns involving multiple segments of the same fault or segments of multiple fault zones. These results further support the conclusion of dePolo et al. (1991) that commonly used fault-segmentation models (cf. Schwartz and Coppersmith, 1984) may not be completely adequate for evaluating the potential for large surface-faulting events in the Basin and Range province. Owing to the difficulty in discriminating distributive fault events in the paleoseismic record, it may not be possible to confidently identify these rupture patterns in seismic hazard studies.

Slip rate is commonly used to determine seismic energy (moment) release rate on faults and to estimate earthquake recurrence in probabilistic seismic hazard analyses (Youngs and Coppersmith, 1985; Panel on Seismic Hazard Analyses, 1988). The preferred 0.4–0.5 mm/yr rate estimated for the Monte Cristo Valley fault zone is not considered a high (>1 mm/yr) slip rate (Slemmons and dePolo, 1986), and it suggests that slip rate may not be a reliable criterion for characterizing seismic hazard in the Walker Lane region. Other adjacent historical fault zones also have comparable low to moderate slip rates. Machette et al. (1993) inferred a low slip rate for the 1915 Pleasant Valley fault zone (Fig. 1A), and late Quaternary slip rates in the 1954 Dixie Valley and 1954 Fairview Peak rupture zones were inferred to have been 0.2–0.5 mm/yr and <0.1 mm/yr, respectively (Bell and Katzer, 1990; Bell, 1993). These slip rates are as much as an order of magnitude lower than other high-slip-rate faults that have not ruptured historically. In the northern part of the region, the Pyramid Lake and Honey Lake faults (Fig. 1A) have slip rates of >1 mm/yr and 1.1–2.6 mm/yr, respectively (Anderson and Hawkins, 1984; Wills and Borchardt, 1993). Trenching studies along the eastern Sierra Nevada range front indicate a slip rate of >1–2 mm/yr for the Genoa fault (Ramelli et al., 1996), and Reheis and Sawyer (1997) reported a 2–3 mm/yr slip rate on the Fish Lake Valley fault.

We speculate that either of two alternative fault models that include additional, unrecognized subevents can account for the complicated pattern of surface faulting and for a factor-of-two-to-three disparity between the instrumentally and geologically determined seismic moments. A three-event model places an additional subevent on a northwest-striking fault beneath Monte Cristo and Stewart Valleys, and a four-event model hypothesizes two additional subevents, each occurring on north-striking faults in Stewart and Monte Cristo Valleys. Either of the alternative three- and four-event models could adequately account for the extensive primary surface faulting in Monte Cristo Valley. The addition of a third or fourth subevent would increase the total instrumental seismic moment of the earthquake to $4.3–4.7 \times 10^{26}$ dyne · cm and correspond to a

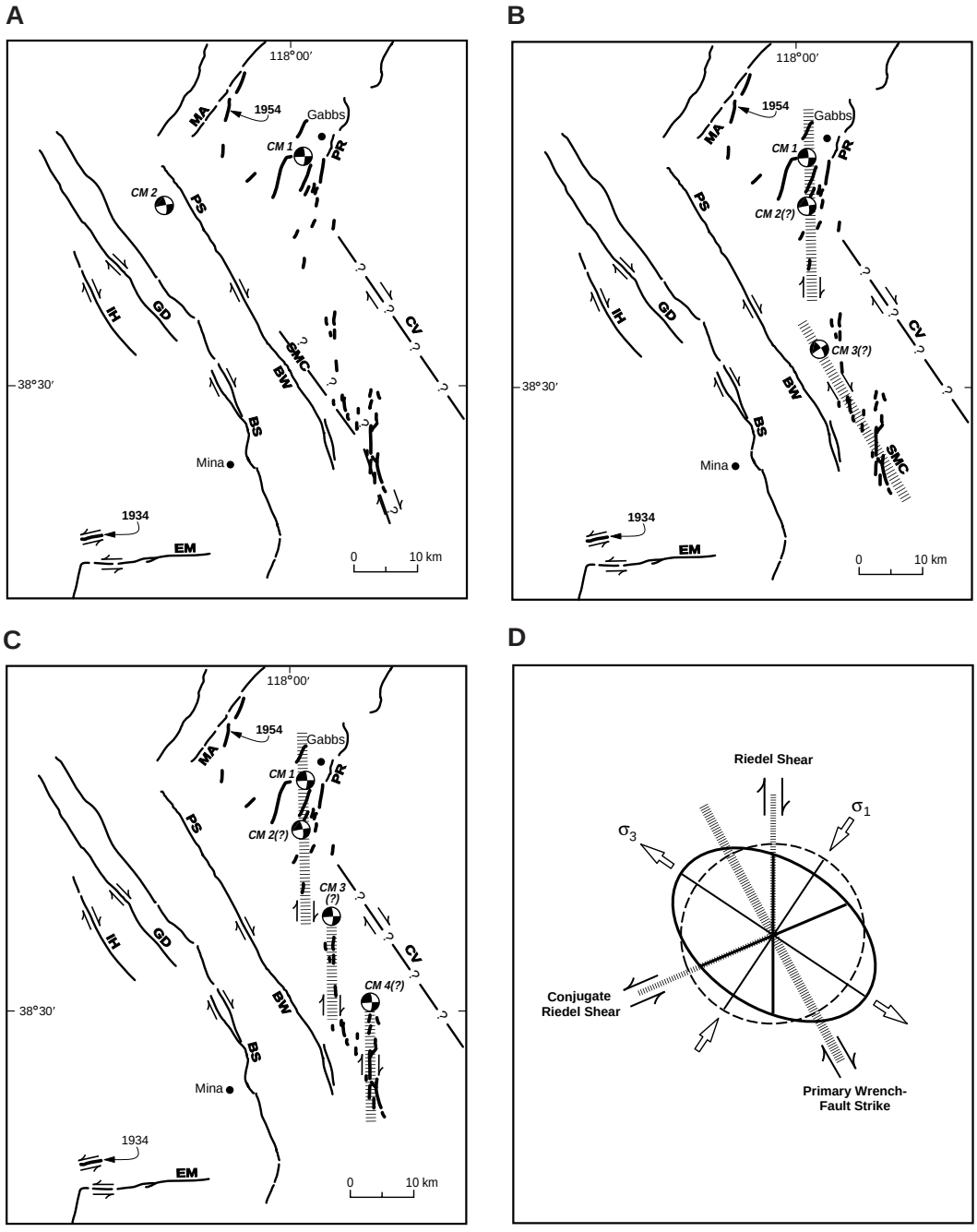

Figure 10. Alternative tectonic models for the 1932 Cedar Mountain fault rupture. The common base map shows the 1932 ruptures (heavy fault lines) and principal late Cenozoic faults (labels explained in Fig. 1B). (A) Two-event model based on original location of epicenters (Doser, 1988): the main event (CM 1) in Gabbs Valley and a second subevent (CM 2) near the Petrified Spring fault. (B) Three-event model based on hypothesizing one additional subevent in Stewart and Monte Cristo Valleys. The CM 2 subevent of Doser (1988) is relocated to Gabbs Valley. The third subevent (CM 3) has inferred right-lateral motion on a northwest-oriented nodal plane and is placed on a postulated northwest-striking fault (Stewart–Monte Cristo Valley fault) beneath Stewart and Monte Cristo Valleys. (C) Four-event model based on hypothesizing two subevents in Stewart and Monte Cristo Valleys. The third (CM 3) and fourth (CM 4) subevents are placed on postulated north-striking faults underlying each of the two valleys. Inferred motion on each fault is right-lateral along north-striking nodal planes. (D) Diagrammatic strain ellipse illustrating Riedel right-lateral simple-shear relationships oriented for the central Nevada region. The ellipse shows the relationships among the primary, northwest-trending, wrench-fault orientation (here assumed to parallel the Walker Lane faults); the north-trending, right-lateral Riedel (synthetic) shear orientation; and the east-northeast–trending, left-lateral conjugate Riedel (antithetic) shear orientation. Modified from Wilcox et al. (1973).

TABLE 3. COMPARISON OF SEISMIC MOMENTS (M_o) AND MOMENT MAGNITUDES (M_w) FROM SINGLE-EVENT (GIANELLA AND CALLAGHAN, 1934A, 1934B), TWO-EVENT (DOSER, 1988), AND ALTERNATIVE THREE- AND FOUR-EVENT MODELS (THIS STUDY)

Model	Subevents	Fault length (km)	Average displacement (m)*	M_o (dyne · cm)†	M_w§
Single-event	One event	60	2	5.4×10^{26} (geologic M_o)	7.1
Two-event	Subevent 1	18	1.3	$11.2 \pm 2 \times 10^{25}$	
	Subevent 2	12	1.8	$8.5 \pm 2.2 \times 10^{25}$	
				1.97×10^{26} (instrumental M_o)	6.8
Three-event	Subevent 1	18	1.3	$11.2 \pm 2 \times 10^{25}$	
	Subevent 2	12	1.8	$8.5 \pm 2.2 \times 10^{25}$	
	Subevent 3	30	2	2.7×10^{26}	
				4.67×10^{26}	7.1
Four-event	Subevent 1	18	1.3	$11.2 \pm 2 \times 10^{25}$	
	Subevent 2	12	1.8	$8.5 \pm 2.2 \times 10^{25}$	
	Subevent 3	17	1	7.6×10^{25}	
	Subevent 4	17	2	1.5×10^{26}	
				4.26×10^{26}	7.1

*Single- and two-event values from Doser (1988); three- and four-event values are average displacement determined from field measurements and Figure 4.
†Single- and two-event values from Doser (1988); three- and four-event values are based on 15 km seismogenic depth, and $\mu = 3 \times 10^{11}$ dyne · cm^2.
§Calculated from $M_w = 2/3 \log M_o - 10.7$ (Hanks and Kanamori, 1979).

moment magnitude (M_w) of 7.1 (Table 3), a value that is close to the original surface-wave magnitude (M_s 7.2). Further wave-form modeling of the 1932 seismograms could resolve which of these models is correct.

The 1932 Cedar Mountain earthquake provides a modern analogue for interpreting late Cenozoic structural and tectonic relationships within the Walker Lane region. The results of this study indicate that Riedel shear relationships can explain the pattern of surface faulting associated with the 1932 event. Right-lateral simple-shear relationships are consistent with Cenozoic kinematic models proposed for the central Walker Lane (Hardyman, 1984; Hardyman and Oldow, 1991), and such relationships may be applicable for contemporary tectonic models elsewhere in the Walker Lane region.

ACKNOWLEDGMENTS

J. C. Yount and P. A. Glancy contributed to the regional Quaternary stratigraphic studies. We thank reviewers T. Gardner, S. McGill, J. Savage, and T. Sawyer for their very helpful comments. This study was supported by funding from the Nevada Nuclear Waste Project Office to the Center for Neotectonic Studies, University of Nevada, Reno. Part of the research was conducted while J. W. Bell was on sabbatical leave at the Institut de Physique du Globe, Université Louis-Pasteur de Strasbourg, France.

REFERENCES CITED

Anderson, L. W., and Hawkins, F. F., 1984, Recurrent Holocene strike-slip faulting, Pyramid Lake fault zone, western Nevada: Geology, v. 12, p. 681–684.

Bell, J. W., 1993, Behavior of late Quaternary and historical faults in the western Basin and Range province: Geological Society of America Abstracts with Programs, v. 25, no. 5, p. 8.

Bell, J. W., 1995, Quaternary geologic map of the Mina quadrangle: Nevada Bureau of Mines and Geology Field Studies Map 10, scale 1:24 000, 1 sheet.

Bell, J. W., and Katzer, T., 1990, Timing of late Quaternary faulting in the 1954 Dixie Valley earthquake area, central Nevada: Geology, v. 18, p. 662–625.

Benson, L. V., Currey, D. R., Dorn, R. I., Lajoie, K. R., Oviatt, C. G., Robinson, S. W., Smith, G. I., and Stine, S., 1990, Chronology of expansion and contraction of four Great Basin lake systems during the past 35 000 years: Palaeogeography, Palaeoclimatology, Palaeoecology, v. 78, p. 241–286.

Brune, J. N., 1968, Seismic moment, seismicity, and rate of slip along major fault zones: Journal of Geophysical Research, v. 73, p. 777–784.

Bull, W. B., 1991, Geomorphic responses to climatic change: New York, Oxford University Press, 326 p.

Byerly, P., 1935, The first preliminary waves of the Nevada earthquake of December 20, 1932: Seismological Society of America Bulletin, v. 25, p. 161–168.

Carr, W. J., 1984, Regional structural setting of Yucca Mountain, southwestern Nevada, and late Cenozoic rates of tectonic activity in part of the southwestern Great Basin, Nevada and California: U.S. Geological Survey Open-File Report 84–854, 109 p.

Caskey, S. J., Wesnousky, S. G., Zhang, P., and Slemmons, D. B., 1996, Surface faulting of the 1954 Fairview Peak (M_s 7.2) and Dixie Valley (M_s 6.8) earthquakes, central Nevada: Seismological Society of America Bulletin, v. 86, p. 761–787.

Chichagova, O. A., and Cherkinsky, A. E., 1993, Problems in radiocarbon dating of soils: Radiocarbon, v. 35, p. 351–362.

Christie-Blick, N., and Biddle, K. T., 1985, Deformation and basin formation along strike-slip faults, *in* Biddle, K. T., and Christie-Blick, N., eds., Strike-slip deformation, basin formation, and sedimentation: Society of Economic Paleontologists and Mineralogists Special Publication 37, p. 1–34.

dePolo, C. M., Clark, D. G., Slemmons, D. B., and Ramelli, A. R., 1991, Historical surface faulting in the Basin and Range province, western North America: Implications for fault segmentation: Journal of Structural Geology, v. 13, p. 123–136.

Doser, D. I., 1988, Source parameters of earthquakes in the Nevada seismic zone, 1915–1943: Journal of Geophysical Research, v. 93, p. 15001–15015.

Ekren, E. B., and Byers, F. M., 1984, The Gabbs Valley range—A well-exposed segment of the Walker Lane in west-central Nevada, *in* Lintz, J., ed., Western geological excursions, Volume 4: Geological Society of America, 1984 Annual Meeting, Reno, Nevada, Field Trip Guidebook, p. 203–215.

Ekren, E. B., Bucknam, R. C., Carr, W. J., Dixon, G. L., and Quinlivan, W. D., 1976, East-trending structural lineaments in central Nevada: U.S. Geological Survey Professional Paper 986, 16 p.

Forman, S. L., 1989, Applications and limitations of thermoluminescence to date Quaternary sediments: Quaternary International, v. 1, p. 47–59.

Forman, S. L., Machette, M. N., Jackson, M. E., and Maat, P. 1989, An evaluation of thermoluminescence dating of paleoearthquakes on the American Fork segment, Wasatch fault zone, Utah: Journal of Geophysical Research, v. 94, p. 1622–1630.

Fridrich, C. J., 1998, Tectonic evolution of the Crater Flat basin, Yucca Mountain region, Nevada: U.S. Geological Survey Open-File Report 98–33, 43 p.

Geyh, M. A., Benzler, J. H., and Roeschmann, G., 1971, Problems of dating Pleistocene and Holocene soils by radiometric methods, *in* Yaalon, D. H., ed., Paleopedology—Origin, nature and dating of paleosols: Jerusalem, International Society of Soil Science, Israel University Press, p. 63–75.

Gianella, V. P., and Callaghan, E., 1934a, The Cedar Mountain, Nevada, earthquake of December 20, 1932: Seismological Society of America Bulletin, v. 24, p. 345–377.

Gianella, V. P., and Callaghan, E., 1934b, The earthquake of December 20, 1932, at Cedar Mountain, Nevada, and its bearing on the genesis of Basin Range structure: Journal of Geology, v. 42, p. 1–22.

Gile, L. H., 1975, Holocene soils and soil-geomorphic relations in an arid region of southern New Mexico: Quaternary Research, v. 5, p. 321–360.

Gile, L. H., Peterson, F. F., and Grossman, R. B., 1966, Morphological and genetic sequences of carbonate accumulation in desert soils: Soil Science, v. 101, p. 347–360.

Hanks, T. C., and Kanamori, H., 1979, A moment magnitude scale: Journal of Geophysical Research, v. 84, no. B5, p. 2348–2350.

Hardyman, R. F., 1984, Strike-slip, normal, and detachment faults in the northern Gillis Range, Walker Lane of west-central Nevada, *in* Lintz, J., ed., Western Geological Excursions, Volume 4: Geological Society of America, 1984 Annual Meeting, Reno, Nevada, Field Trip Guidebook, p. 184–199.

Hardyman, R. F., and Oldow, J. S., 1991, Tertiary tectonic framework and Cenozoic history of the central Walker Lane, Nevada, *in* Proceedings, Symposium on geology and ore deposits of the Great Basin, Reno, April, 1990: Reno, Nevada, Geological Society of Nevada, p. 279–301.

Hardyman, R. F., McKee, E. H., Snee, L. W., and Whitebread, D. H., 1992, The Camp Terrill and Dicalite Summit faults: Two contrasting examples of detachment faults in the central Walker Lane, western Nevada, *in* Proceedings, Walker Lane Symposium, Reno, April, 1992: Reno, Nevada, Geological Society of Nevada, p. 93–113.

Janssen, B., 1995, Modélisation numerique de l'extension de la croûte terrestre avec des examples du Basin and Range, États-Unis [Ph.D. thesis]: Strasbourg, France, Université Louis-Pasteur de Strasbourg, 170 p.

Johnson, A., Fleming, R. W., and Cruikshank, K. M., 1994, Shear zones along long, straight traces of fault zones dur-

ing the 28 June 1992 Landers, California, earthquake: Seismological Society of America Bulletin, v. 84, p. 499–510.
Locke, A., Billingsley, P. R., and Mayo, E. B., 1940, Sierra Nevada tectonic patterns: Geological Society of America Bulletin, v. 51, p. 513–540.
Machette, M. N., Personius, S.F., and Nelson, A. R., 1990, Paleoseismology of the Wasatch fault zone: A summary of recent investigations, interpretations, and conclusions: U.S. Geological Survey Professional Paper 1500-A, 71 p.
Machette, M. N., Haller, K. M., and Berryman, K. R., 1993, Prehistoric movement along the 1915 Pleasant Valley fault zone and implications for the central Nevada seismic belt: Geological Society of America Abstracts with Programs, v. 25, no. 5, p. 112.
Molinari, M. P., 1984, Late Cenozoic geology and tectonics of Stewart and Monte Cristo Valleys, west-central Nevada [master's thesis]: Reno, Nevada, University of Nevada, Reno, 124 p.
Moody, J. D., and Hill, M. J., 1956, Wrench-fault tectonics: Geological Society of America Bulletin, v. 67, p. 1207–1246.
Naylor, M. A., Mandl, G., and Sijpesteijn, C. H. K., 1986, Fault geometries in basement-induced wrench faulting under different initial stress states: Journal of Structural Geology, v. 8, p. 737–752.
North American Commission on Stratigraphic Nomenclature, 1983, North American stratigraphic code: American Association of Petroleum Geologists Bulletin, v. 67, p. 841–875.
O'Leary, D. W., 1996, Synthesis of tectonic models for the Yucca Mountain area, *in* U.S. Geological Survey, Seismotectonic framework and characterization of faulting at Yucca Mountain, Nevada, Chapter 8: Unpublished report to the U.S. Department of Energy, p. 8-1–8-153.
Orlova, L. A., and Panychev, V. A., 1993, The reliability of radiocarbon dating buried soils: Radiocarbon, v. 35, p. 369–377.
Panel on Seismic Hazard Analysis, 1988, Probabilistic seismic hazard analysis: Washington, D.C., National Academy Press, 97 p.
Pearthree, P., 1990, Geomorphic analysis of young faulting and fault behavior in central Nevada [Ph.D. thesis]: Tucson, University of Arizona, 212 p.
Peterson, F. F., Bell, J. W., Dorn, R. I., Ramelli, A. R., and Ku, T. L., 1995, Late Quaternary geomorphology and soils in Crater Flat, Yucca Mountain area, southern Nevada: Geological Society of America Bulletin, v. 107, p. 379–395.
Ramelli, A. R., Bell, J. W., and dePolo, C. M., 1996, Late Holocene activity of the Genoa fault, western Nevada: Geological Society of America Abstracts with Programs, v. 28, no. 5, p. 103.
Reheis, M. C., and Sawyer, T. L., 1997, Late Cenozoic history and slip rates of the Fish Lake Valley, Emigrant Peak, and Deep Springs fault zones, Nevada and California: Geological Society of America Bulletin, v. 109, p. 280–299.
Riedel, W., 1929, Zur mechanik geologischer Brucherscheinungen: Zentralblatt für Mineralogie, Geologie und Palaeontologie Abhandlung B, p. 354–368.
Sarna-Wojcicki, A. M., and Pringle, M. S., Jr., 1992, Laser-fusion $^{40}Ar/^{39}Ar$ ages of the tuff of Taylor Canyon and Bishop tuff, California–western Nevada: EOS (Transactions, American Geophysical Union), v. 73, p. 633.
Sarna-Wojcicki, A. M., Bowman, H. R., Meyer, C. E., Russell, P. C., Woodward, M. J., McCoy, G., Rowe, J. J., Baedecker, P. A., Asaro, F., and Michael, H., 1984, Chemical analyses, correlations, and ages of upper Pliocene and Pleistocene ash layers of east-central and southern California: U.S. Geological Survey Professional Paper 1293, 40 p.
Sarna-Wojcicki, A. M., Lajoie, K. R., Meyer, C. E., Adam, D. P., Robinson, S. W., and Anderson, R. S., 1988, Tephrochronologic studies of sediment cores from Walker Lake, Nevada: U.S. Geological Survey Open-File Report 88–548, 25 p.
Savage, J. C., Lisowski, M., Svarc, S. L., and Gross, W. K., 1995, Strain accumulation across the central Nevada seismic belt: Journal of Geophysical Research, v. 100, p. 20257–20269.
Schwartz, D. P., and Coppersmith, K. J., 1984, Fault behavior and characteristic earthquakes: Examples from the Wasatch and San Andreas fault zones: Journal of Geophysical Research, v. 89, p. 5681–5698.
Sieh, K., and Bursik, M., 1986, Most recent eruptions of the Mono Craters, eastern central California: Journal of Geophysical Research, v. 91, p. 12539–12571.
Slemmons, D. B., 1957, Geological effects of the Dixie Valley–Fairview Peak, Nevada, earthquakes of December 16, 1954: Seismological Society of America Bulletin, v. 47, p. 353–375.
Slemmons, D. B., and dePolo, C. M., 1986, Evaluation of active faulting and associated hazards, *in* Active tectonics: Washington, D.C., National Academy Press, National Research Council, Panel on Active Tectonics, p. 45–62.
Soil Survey Staff, 1975, Soil taxonomy: Washington, D.C., U.S. Government Printing Office, U.S. Department of Agriculture Handbook 436, 746 p.
Stewart, J. H., 1988, Tectonics of the Walker Lane belt, western Great Basin: Mesozoic and Cenozoic deformation in a zone of shear, *in* Ernst, W. G., ed., Metamorphism and crustal evolution of the western United States, Rubey Volume VII: Englewood Cliffs, New Jersey, Prentice-Hall, p. 684–713.
Stuiver, M., and Reimer, P. J., 1993, Extended ^{14}C database and revised CALIB 3.0 ^{14}C age calibration program: Radiocarbon, v. 35, p. 215–230.
Sylvester, A. G., 1988, Strike-slip faults: Geological Society of America Bulletin, v. 100, p. 1666–1703.
Tchalenko, J. S., 1970, Similarities between shear zones of different magnitudes: Seismological Society of America Bulletin, v. 81, p. 1625–1640.
Tchalenko, J. S., and Ambraseys, N. N., 1970, Structural analysis of the Dasht-e Bayaz (Iran) earthquake fractures: Geological Society of America Bulletin, v. 81, p. 41–60.
U.S. Department of Energy, 1988, Site characterization plan, Yucca Mountain Site, Nevada Research and Development Area, Nevada: Washington, D.C., U.S. Department of Energy Office of Civilian Radioactive Waste Management, Volumes I–VII, no consecutive pagination.
Wallace, R. E., 1984, Patterns and timing of late Quaternary faulting in the Great Basin province and relation to some regional tectonic features: Journal of Geophysical Research, v. 89, p. 5763–5769.
Wallace, R. E., 1987, Grouping and migration of surface faulting and variations in slip rates on faults in the Great Basin: Seismological Society of America Bulletin, v. 77, p. 868–876.
Wells, D. L., and Coppersmith, K. J., 1994, New empirical relationships among magnitude, rupture length, rupture width, rupture area, and surface displacement: Seismological Society of America Bulletin, v. 84, p. 974–1002.
Whitebread, D. H., and John, D. A., 1982, Geologic map of the Tonopah 1° × 2° quadrangle, central Nevada: U.S. Geological Survey Map MF-1877-A, scale 1:250 000, 1 sheet, 13 p. text.
Wilcox, R. E., Harding, T. P., and Seely, D. R., 1973, Basic wrench tectonics: American Association of Petroleum Geologists Bulletin, v. 57, p. 74–96.
Wills, C. J., and Borchardt, G., 1993, Holocene slip rate and earthquake recurrence on the Honey Lake fault zone, northeastern California: Geology, v. 21, p. 853–856.
Wintle, A. G., and Huntley, D. J., 1982, Thermoluminescence dating of sediments: Quaternary Science Reviews, v. 1, p. 31–53.
Wood, S. H., 1977, Distribution, correlation, and radiocarbon dating of late Holocene tephra, Mono and Inyo Craters, eastern California: Geological Society of America Bulletin, v. 88, p. 89–95.
Youngs, R. R., and Coppersmith, K. J., 1985, Implications of fault slip rates and earthquake recurrence models to probabilistic seismic hazard estimates: Seismological Society of America Bulletin, v. 75, p. 939–964.

MANUSCRIPT RECEIVED BY THE SOCIETY APRIL 15, 1997
REVISED MANUSCRIPT RECEIVED SEPTEMBER 24, 1998
MANUSCRIPT ACCEPTED OCTOBER 23, 1998

Printed in U.S.A.